ANALYSIS OF NEUTRINO INTERACTIONS IN THE OPERA EXPERIMENT

A THESIS SUBMITTED TO
THE GRADUATE SCHOOL OF NATURAL AND APPLIED SCIENCES
OF
MIDDLE EAST TECHNICAL UNIVERSITY

BY

MUSTAFA KAMIŞCIOĞLU

IN PARTIAL FULFILLMENT OF THE REQUIREMENTS
FOR
THE DEGREE OF MASTER OF SCIENCE
IN
PHYSICS

JANUARY 2012

Approval of the thesis:

ANALYSIS OF NEUTRINO INTERACTIONS IN THE OPERA EXPERIMENT

submitted by **MUSTAFA KAMIŞCIOĞLU** in partial fulfillment of the requirements for the degree of **Master of Science in Physics Department, Middle East Technical University** by,

Prof. Dr. Canan Özgen _____
Dean, Graduate School of **Natural and Applied Sciences**

Prof. Dr. Mehmet T. Zeyrek _____
Head of Department, **Physics**

Prof. Dr. Ali Murat Güler _____
Supervisor, **Physics Dept., METU**

Examining Committee Members:

Prof. Dr. Ramazan Sever
Physics Dept., METU _____

Prof. Dr. Ali Murat Güler
Physics Dept., METU _____

Prof. Dr. Atalay Karasu
Physics Dept., METU _____

Prof. Dr. Bayram Tekin
Physics Dept., METU _____

Prof. Dr. Ali Ulvi Yılmazer
Physics Engineering Dept., Ankara University _____

Date: _____

I hereby declare that all information in this document has been obtained and presented in accordance with academic rules and ethical conduct. I also declare that, as required by these rules and conduct, I have fully cited and referenced all material and results that are not original to this work.

Name, Last Name: MUSTAFA KAMIŞCIOĞLU

Signature :

ABSTRACT

ANALYSIS OF NEUTRINO INTERACTIONS IN THE OPERA EXPERIMENT

Kamışcıoğlu, Mustafa
M.Sc., Department of Physics
Supervisor : Prof. Dr. Ali Murat Güler

January 2012, 49 pages

OPERA stands for Oscillation Project with Emulsion t-Racking Apparatus. The main goal of the OPERA experiment is to search for ν_τ appearance in almost pure ν_μ beam. The detector is located at Gran Sasso, 730 km away from the neutrino source, at CERN. In this thesis, the reconstruction efficiency and purity of neutrino interactions in the OPERA target have been studied by using Monte Carlo simulation. The efficiency of primary vertex reconstruction for ν_μ Charge Current (CC) events is estimated as 83.2%. The main source of inefficiency is due to Quasi-elastic like topologies in which only one track is reconstructed. The purity of primary vertex tracks is found to be 99%. On the other hand, the reconstruction efficiency for ν_μ CC charm events is estimated to be 90.2%, while the purity of the primary tracks is 67%. The low purity is due the fact that the secondary vertex tracks are wrongly assigned in the primary vertex. This spoils the purity.

Keywords: Neutrino, Neutrino Oscillation, Nuclear Emulsion, Charm Particle

ÖZ

OPERA DENEYİNDE NÖTRİNO ETKİLEŞİMLERİNİN ANALİZİ

Kamışcıoğlu, Mustafa
Yüksek Lisans, Fizik Bölümü
Tez Yöneticisi : Prof. Dr. Ali Murat Güler

Ocak 2012, 49 sayfa

OPERA kelimesi "Oscillation Project with Emulsion t-Racking Apparatus" olarak adlandırılan deneyin kısaltmasıdır. Deneyin amacı; CERN'den gönderilen ve neredeyse saf müon nötrinosu içeren demette, görünür modda tau nötrinosunu araştırmaktır. Detektör CERN'den 730 km uzaklıkta bulunan Gran Sasso'da yer almaktadır. Bu tez calışmanında, Monte Carlo (MC) simülasyonları kullanılarak yapılandırılmış OPERA dedektöründeki nötrino etkileşmelerinin verim ve saflık durumları çalışılmıştır. Müon nötrino CC olaylar için birinci vertex yapılandırılmış verimi %83.2 olarak bulunmuştur. Verim kaybının temel nedeni bir parçacık izinin yapılandırıldığı quasi elastic topolojilerden kaynaklanmaktadır. Çalışmada birinci vertex izlerin saflığı %99 olarak hesaplanmıştır. Öte yandan müon nötrino CC Charm olayları için yapılandırma verimi %90.2 olarak bulunurken, birincil izlerin saflığı %67 olarak bulunmuştur. Düşük saflığın sebebi, ikinci vertex izlerinin birinci vertexe eklenmesinden kaynaklanmaktadır. Bu durum saflığı bozmaktadır.

Anahtar Kelimeler: Nötrino, Nötrino Salınımları, Nükleer Emülsiyon, Charm Parçacığı

To my family

ACKNOWLEDGMENTS

I would like to express my sincere thanks to my supervisor, Prof. Dr. Ali Murat Güler, for giving me an opportunity to involve in the OPERA Collaboration and for his valuable guidance and support throughout this research.

I am deeply indebted to my family and all of my friends for their endless supports, love and believe in me.

I would also like to express my gratitude to the group members of METU OPERA for their friendship and helps.

I would like to thank all the people in Gran Sasso Scanning Laboratory for their helps and support.

I would like to thank to INFN for the financial support during my stays in LNGS.

I would also like to thank TÜBİTAK (project no: 108T324) for providing a scholarship.

TABLE OF CONTENTS

LIST OF TABLES

TABLES

LIST OF FIGURES

FIGURES

CHAPTER 1

INTRODUCTION

Neutrinos still hold their mystery, although more than half century have passed since they were detected through various experiments and methods. We know today, that neutrinos are neutral leptons with a tiny mass and that there exist only three types of neutrinos called as electron-neutrino, muon-neutrino and tau-neutrino; ν_e, ν_μ, ν_τ. Neutrinos play very important role in astrophysics and cosmology. They carry information about the core of the sun, core-collapse supernova. They could be responsible for the origin of the baryon asymmetry of the universe. On the theoretical side non-zero neutrino mass represents clear indication of physics beyond the Standard Model.

In 1914, J. Chadwick observed that the electron emitted in beta decay has a continuous spectrum, unlike what happen in α and γ decays. However, if all the disintegration energy is spent for the beta particle, the spectrum must be monochromatic. Therefore it seemed that energy is not conserved in beta decay. In 1930, W. Pauli suggested that the missing energy in beta decay can be explained by introducing a neutral and massless or a small massive particle which was called neutron. Three years later E. Fermi renamed it as neutrino.

In 1956, anti-electron neutrino was first experimentally observed by F. Reines and C. Cowan at Savannah River Nuclear Reactor. F. Reines was awarded with Nobel Prize in 1995 for this discovery [1].

In 1962, muon neutrino was discovered in Brookhaven National Laboratories by L. Lederman, M. Schwartz, J. Steinberger. They were awarded with the 1988 Nobel Prize in Physics [2].

In 2000, tau neutrino was discovered in a direct observation for the first time by the DONUT (Direct Observation of the NU Tau) collaboration [3].

The measurement of the Z^0 line width at LEP showed that there are only three types of neutrinos with masses less than 45 GeV [4].

Neutrino oscillation is one of the most challenging phenomena in physics. Many experiments have searched neutrino oscillations using different sources and techniques. The first indication of neutrino oscillations came from the solar neutrino flux measurements which was started by R. Davis in Homestake. There are convincing results for neutrino oscillations reported by several experiments like Super-Kamiokande [5], K2K [6], KAMLAND [7], SNO [8], T2K [9], MINOS [10]. The final proof for neutrino oscillations would be direct observation of ν_τ in almost pure ν_μ beam. This is the main motivation of the OPERA experiment.

This thesis work organized as follows: In Chapter 2, interactions of neutrino with matter will be explained. It is followed by the theory of neutrino oscillation and some of the dedicated experiments. Then, neutrino induced charm production mechanism and experimental results will be given. In Chapter 3, all components of the OPERA detector, their functions and physics performances are represented. In Chapter 4, a Monte Carlo simulation to estimate the reconstruction efficiency of $\nu_\mu CC$ and $\nu_\mu CC - Charm$ events will be presented. Finally, results will be discussed in Chapter 5.

CHAPTER 2

NEUTRINO INTERACTIONS

Neutrino interactions are described by the Standard Model of particle physics [11]. In Standard Model, neutrinos are defined as massless neutral leptons. Therefore, they interact only weakly with matter. The weak interaction takes place between all fundamental particles except gluons and photon. According to Standard Model, weak interaction occurs either by the exchange of Z^0 neutral boson or $W^{\pm}$ charged vector bosons. These bosons were discovered at CERN(European Council for Nuclear Research) in 1983 [12]. Their masses are about 100 of proton mass.

Depending on the exchange vector bosons, neutrino interactions are classified as charged current (CC) when $W^{\pm}$ exchange takes place or neutral current (NC) interaction when Z^0 exchange takes place:

$$\nu_\mu + N \rightarrow \nu_\mu + X \;\; (NC) \tag{2.1}$$

$$\nu_\mu + N \rightarrow \mu^- + X \;\; (CC) \tag{2.2}$$

where N is nucleon and X stands for outgoing hadrons. Feynmann diagrams for CC and NC interactions are shown in Figure 2.1. Unlikely to other interactions, weak interaction can do flavour changing transitions. For example, up quark can change into down quark. Flavour changing transitions are very important for several issues which will be discussed later.

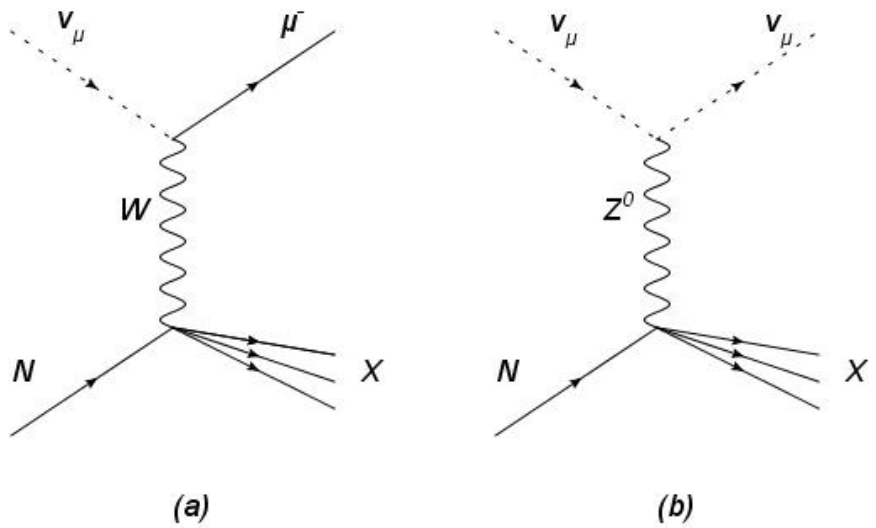

Figure 2.1: (a) CC neutrino interaction (b) NC neutrino interaction.

2.1 Neutrino Interactions with matter

Neutrino interactions with nucleon can be categorized in four basic types depending on the energy of incoming neutrino. These interactions are elastic scattering, quasi-elastic scattering (QE), resonances (RES) and deep inelastic scattering (DIS) as shown in Figure 2.2.

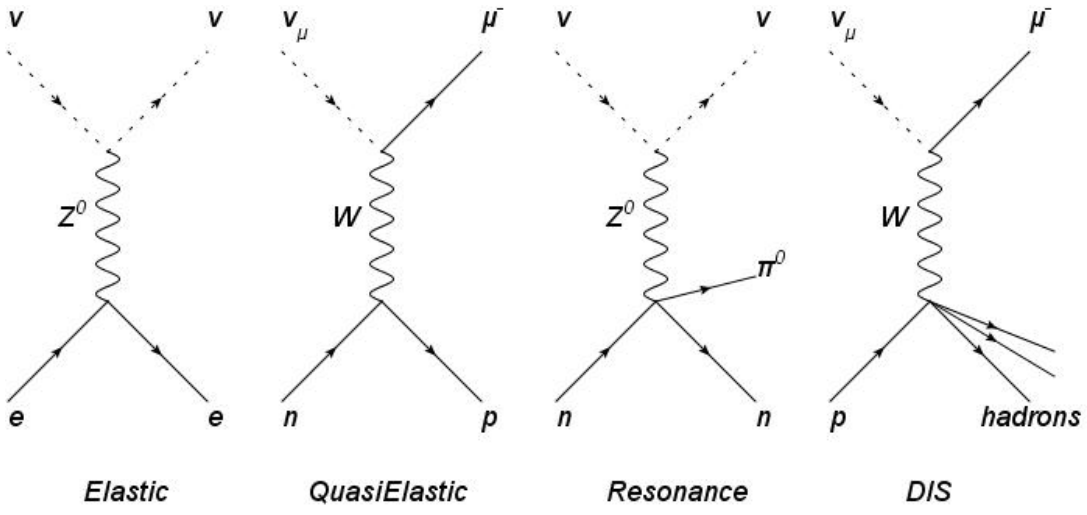

Figure 2.2: Types of neutrino interactions with matter.

Elastic Scattering: Elastic scattering is like a repulsion of two electrons where they just feel the force not colliding each other. In this scattering incoming and outgoing particles are

the same. For example,

$$\nu_e + n \rightarrow \nu_e + n, \tag{2.3}$$

where ν_e can scatter with neutron which will not break up or not jump into excited states later. These interactions are difficult to detect since outgoing nucleon does not have enough momentum to be identified.

Quasi-elastic Scattering: It is similar to elastic scattering where CC interaction takes place. In quasi-elastic scattering one of the target quarks change its flavour due to the exchange of W boson. For example,

$$\nu_e + n \rightarrow e^- + p. \tag{2.4}$$

Quasi-elastic scattering contribution is maximum when E_{ν_e}< 2 GeV. This interaction is important for neutrino oscillation experiments since one can determine the true neutrino energy by measuring muon and proton energy.

Resonance: In resonance, the target becomes Δ which decays and emits a single pion. In the case of a small momentum exchange with nucleon, pion is produced diffractively in the forward direction. A single pion production in NC interactions is important in neutrino oscillation experiments since they form the main background for the oscillation signal.

Deep Inelastic Scattering: It is a characteristic interaction for high energy neutrinos, E_ν> 1 GeV. This interaction can be described as a reaction between neutrino and partons in the nucleons. The energy dependence of cross sections for these interactions is shown in the Figure 2.3. The sum of QE, RES and DIS cross sections gives the total cross section. Since CNGS neutrino beam has a mean energy of 17 GeV, the DIS cross section has the largest contribution. DIS is possible through CC or NC interaction. In CC interaction there must be adequate CM energy in order to produce charged leptons. This threshold energy for τ^- production is about 5.4 GeV.

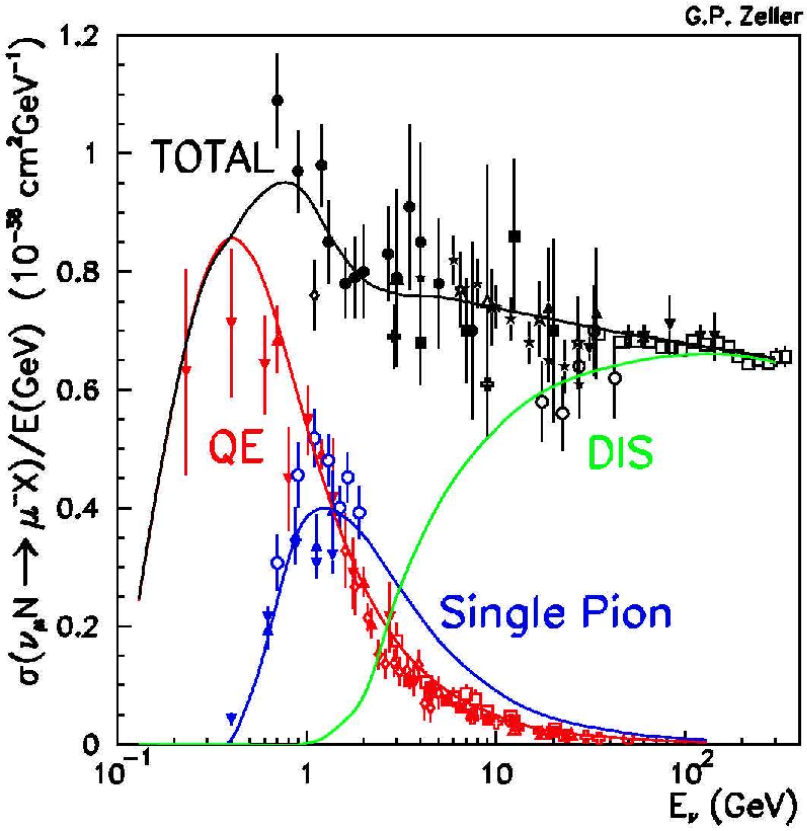

Figure 2.3: Cross section of neutrino-nucleon interactions.

2.2 Neutrino Oscillation

Neutrino astrophysics has a lot of questions about neutrinos whether they have mass or not, can they do flavour oscillation, do they have detectable electromagnetic moments and many other questions. One of the oldest problems in neutrino astrophysics is solar neutrino problem which can be solved by neutrino oscillations as proposed by B. Pontecorvo in 1958 [13].

In Standard Model neutrinos are assumed to be massless Dirac particle without any fundamental reason. However, the theory of neutrino oscillation requires that neutrinos have to be massive. Thus, neutrino oscillation cannot be explained in Standard Model, the neutrino oscillation is physics beyond the Standard Model. In order to observe neutrino oscillation the following conditions must be fulfilled:

i) Neutrinos have masses.

ii) They mix among each other.

If neutrinos are massive, there is a set of mass eigenstates denoted by ν_i which describe the evolution of neutrinos in space and time [14]. On the other hand interaction of neutrinos with matter is described by the flavour eigenstates ν_α.

Neutrino flavour state can be defined in terms of mass eigenstates as

$$|\nu_\alpha\rangle = \sum_{i=1} U^*_{\alpha i}|\nu_i\rangle, \tag{2.5}$$

where U is 3×3 unitary leptonic mixing matrix, also known as Pontecorvo, Maki, Nakagawa and Sakata (PMNS) matrix [15]. It is given as

$$\begin{pmatrix} \nu_e \\ \nu_\mu \\ \nu_\tau \end{pmatrix} = \begin{pmatrix} U_{e1} & U_{e2} & U_{e3} \\ U_{\mu 1} & U_{\mu 2} & U_{\mu 3} \\ U_{\tau 1} & U_{\tau 2} & U_{\tau 3} \end{pmatrix} \times \begin{pmatrix} \nu_1 \\ \nu_2 \\ \nu_3 \end{pmatrix}$$

The flavour eigenstates on the left can be written in terms of mass eigenstates on the right multiplied by PMNS matrix. Similarly, the mass eigenstates can be written in terms of the flavour eigenstates as

$$|\nu_i\rangle = \sum_{i=1} U_{\alpha i}|\nu_\alpha\rangle. \tag{2.6}$$

The time evolution of neutrino mass eigenstates can be obtained by using the Schrödinger equation and relativistic energy equation

$$i\hbar\frac{\partial\Psi}{\partial t} = H\Psi = E\Psi, \tag{2.7}$$

$$E^2 = m^2c^4 + p^2c^2. \tag{2.8}$$

In the rest frame of neutrino mass eigenstates, Eqn. 2.7 [1] becomes

[1] Here we have taken $\hbar = c = 1$.

$$i\frac{\partial|\nu_i(\tau_i)\rangle}{\partial\tau} = m_i|\nu_i(\tau_i)\rangle. \tag{2.9}$$

After solving Eqn. 2.9, one gets

$$|\nu_i(\tau_i)\rangle = e^{-im_i\tau_i}|\nu_i(0)\rangle. \tag{2.10}$$

This state is expressed in the center of mass(CM) frame, however it is necessary to express it with measurable quantities in lab frame.

$$\tau = \gamma(t - \nu L), \tag{2.11}$$

where L is the distance from source to detector, ν is neutrino velocity and $\gamma = \frac{1}{\sqrt{1-\frac{\nu^2}{c^2}}}$. After multiplying Eqn. 2.11 with mass m and using $E = \gamma mc^2$ and $p = \gamma m\nu/c$, one obtains

$$m_i\tau_i = E_i t - p_i L. \tag{2.12}$$

For ultra relativistic neutrino one can take momentum as

$$p \approx E(1 - \frac{m^2}{2E^2}). \tag{2.13}$$

After inserting Eqn. 2.13 into Eqn. 2.12, where $t \approx L$, one obtains

$$m_i\tau_i = \frac{m_i^2}{2E}L. \tag{2.14}$$

Then, time evolved neutrino mass eigenstate can be written as

$$|\nu_i(t)\rangle = e^{-i\frac{m_i^2}{2E}L}|\nu_i(0)\rangle. \tag{2.15}$$

By inserting Eqn. 2.15 into Eqn. 2.5, one gets

$$|\nu_\alpha(L)\rangle = \sum_{i=1} U^*_{\alpha i} e^{-i\frac{m_i^2}{2E}L} |\nu_i\rangle. \tag{2.16}$$

If the mass eigenstate $|\nu_i\rangle$ is expressed in terms of flavour eigenstates, Eqn. 2.16 becomes

$$|\nu_\alpha(L)\rangle = \sum_{\beta=1} [\sum_{i=1} U^*_{\alpha i} e^{-i\frac{m_i^2}{2E}L} U_{\beta i}] |\nu_\beta\rangle. \tag{2.17}$$

This equation shows that after propagating a distance L, the $|\nu_\alpha(L)\rangle$ states become superposition of all flavours. Then, neutrino oscillation probability can be computed by taking the square of the amplitude, $\langle\nu_\beta|\nu_\alpha(L)\rangle$.

$$Prob(\nu_\alpha \rightarrow \nu_\beta) = |\langle\nu_\beta|\nu_\alpha(L)\rangle|^2 = \delta_{\alpha\beta} - 4\Sigma U_{\alpha i} U^*_{\beta i} U^*_{\alpha j} U_{\beta j} sin^2(\frac{1.27\Delta m^2_{ij} L}{E}), \tag{2.18}$$

where $\Delta m^2_{ij} = m^2_j - m^2_i$, α and β are flavour indices (e, μ, τ) and i and j are mass eigenstate indices (1, 2, 3). As seen in the Eqn. 2.18, probability depends on the propagation length L and energy of neutrino, E. The probability increases with L, however it decreases with E.

In observing flavour oscillation not only oscillation probability but also neutrino cross section is important. However there is a contradiction in the energy contribution. When energy is low the cross section is relatively small so does the probability however, the oscillation probability is high. On the other hand when energy is high the cross section is relatively large so does interaction probability high however the oscillation probability is low. Thus, whether energy is low or high, the probability is suppressed with a factor. Furthermore, the oscillation probability depends also Δm^2 which is mass squared difference. There are three mass squared differences; Δm^2_{12}, Δm^2_{13} and Δm^2_{23}. The present measurements are consistent with two possibilities for the mass ordering. In normal hierarchy ($\Delta m^2_{31} > 0$), the mass state m_1 has the smallest mass, whereas in the inverted hierarchy ($\Delta m^2_{31} < 0$), state m_3 has the smallest mass. One of the main goal of the upcoming experiments is the determination of the sign of Δm^2_{31}.

The three neutrino oscillation parameter can be determined from a global analysis of neutrino oscillation data from solar, atmospheric reactor and accelerator experiments. The present three-flavour neutrino oscillation parameters is summarized in Table 2.1.

Table 2.1: Present neutrino oscillation parameters [16].

parameter	best fit $\pm 1\sigma$	2σ	3σ
Δm^2_{21} $[10^{-5}\text{eV}^2]$	$7.59^{+0.20}_{-0.18}$	7.24–7.99	7.09–8.19
Δm^2_{31} $[10^{-3}\text{eV}^2]$	2.45 ± 0.09 $-(2.34^{+0.10}_{-0.09})$	$2.28 - 2.64$ $-(2.17 - 2.54)$	$2.18 - 2.73$ $-(2.08 - 2.64)$
$\sin^2\theta_{12}$	$0.312^{+0.017}_{-0.015}$	0.28–0.35	0.27–0.36
$\sin^2\theta_{23}$	0.51 ± 0.06 0.52 ± 0.06	0.41–0.61 0.42–0.61	0.39–0.64
$\sin^2\theta_{13}$	$0.010^{+0.009}_{-0.006}$ $0.013^{+0.009}_{-0.007}$	≤ 0.027 ≤ 0.031	≤ 0.035 ≤ 0.039

2.3 Neutrino Oscillation Experiments

A number of neutrino experiments have searched for neutrino oscillations. They are classified as solar, atmospheric, reactor and accelerator according to neutrino source. The neutrino oscillation experiments can also be classified according to search method as appearance and disappearance experiments. In disappearance mode, the change in the neutrino flux is measured. In the appearance mode, for example in $\nu_e \longrightarrow \nu_\mu$ case, ν_μ interactions are directly observed in the detector. Some of the experiments will be briefly discussed.

Electron Neutrino Oscillation: Electron neutrino oscillation was first studied using solar neutrinos. Solar neutrinos produced as a product of nuclear fusion reactions, called as proton-proton cycle in the sun. However, the energy of all solar neutrinos are not the same since they are produced in different stage of proton-proton cycle as shown in Figure 2.4.

The studies with solar neutrinos go back to 60's. The solar neutrino flux measurement first was done by R. Davis in Homestake [18]. The measured neutrino flux is just one third of the predicted flux. Later this result was verified with the Kamiokande II and other experiments. Neutrinos measured by Kamiokande II experiment are mainly produced in the sun via β decay:

$$^8B \longrightarrow {}^8Be + e^+ + \nu_e \tag{2.19}$$

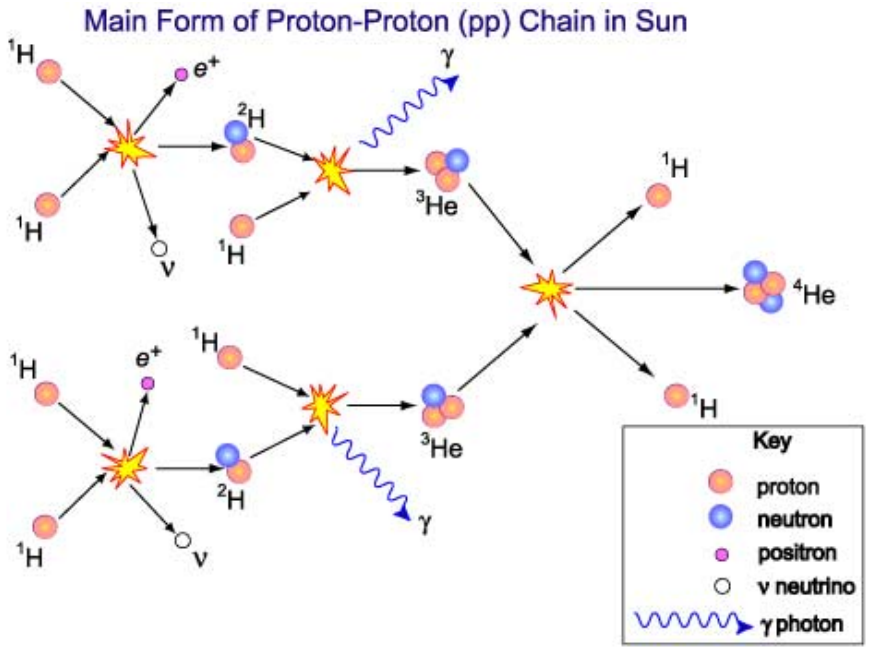

Figure 2.4: Proton-proton cycle [17].

where produced neutrinos have an energy about 7 MeV. Although the experiment reflects the solar neutrino problem, it is sensitive only 10^{-4} of the total solar neutrino flux. In order to cover full spectrum of neutrino flux, the experiment must be sensitive to neutrinos coming from

$$p + p \longrightarrow d + e^{+} + \nu_e \tag{2.20}$$

where neutrino energy is about 0.26 MeV. The Homestake experiment was not able to detect these neutrinos. The experiments with a lower energy threshold proposed at that time are SAGE in Russia and GALLEX in Italy. Both experiments have neutrino interaction threshold of about 0.25 MeV. The studied interaction in these experiments was

$$\nu_e + {}^{71}Ga \rightarrow {}^{71}Ge + e^{-}. \tag{2.21}$$

In SAGE and GALLEX experiments only about 60% of the expected electron neutrino flux was measured. Thus the decrease in the electron neutrino flux was verified. This discrepancy was known as the solar neutrino problem.

Until the end of 2000, many experiments were done however solution of the solar neutrino problem was not clearly stated. In 2002, Sudbury Neutrino Observatory(SNO) settled the solar neutrino problem by demonstrating that it was due to neutrino oscillations. SNO uses heavy water as the detecting medium rather than pure water. Therefore, the SNO experiment can detect the following neutrino interactions:

$$(a)\nu_e + d \longrightarrow e^- + p + p \tag{2.22}$$

$$(b)\nu_x + d \longrightarrow \nu_x + p + n \tag{2.23}$$

$$(c)\nu_x + e^- \longrightarrow \nu_x + e^- \tag{2.24}$$

where x stands for charged leptons (e, μ, τ) and d is the deutron. In (a) observed flux was one third of expected flux, implied that two third of electron neutrino changed to muon or tau neutrinos at the detection point. In (b) cross section was independent of all type of leptons and measured flux was consistent with expectation. In(c) it was observed that cross section is different for ν_e and $\nu_{\mu,\tau}$ and similar to (a), the measured flux below was the expected flux. When each contribution was added, one got the total fluxes as

$$\Phi_{\nu_e}^{SNO} = (1.68 \pm 0.06) \times 10^6 cm^{-2} s^{-1} \tag{2.25}$$

$$\Phi_{\nu_{e,\mu,\tau}}^{SNO} = (4.94 \pm 0.21) \times 10^6 cm^{-2} s^{-1} \tag{2.26}$$

Although the total flux through NC interaction was consistent with Standard Solar Model, $\nu_e CC$ flux is less than expected. This decrease is consistently explained by neutrino oscillation hypothesis.

Muon Neutrino Oscillation: When the energetic protons enter to atmosphere, they interact and produce pions and kaons which then decay into neutrinos through:

$$\pi^- \rightarrow \mu^- + \overline{\nu}_\mu, \tag{2.27}$$

$$\pi^+ \rightarrow \mu^+ + \nu_\mu, \tag{2.28}$$

$$\mu^- \rightarrow e^- + \overline{\nu}_e + \nu_\mu, \tag{2.29}$$

$$\mu^+ \rightarrow e^+ + \nu_e + \overline{\nu}_\mu. \tag{2.30}$$

The Super-Kamiokande experiment is sensitive to atmospheric neutrinos through indirect observation of ν_μ to ν_τ oscillations. The Super-Kamiokande detector, located very deep underground in the Japanese Alps, consists a huge tank of approximately 40 m high and 40 m diameter which is full of very pure water. It is divided into inner and outer part. Inner part has 11,200 photomultiplier tubes. Neutrinos with 1 GeV energy interact with nuclei and produce electrons and muons which then generate Cherenkov light as they propagate in the water. This Cherenkov radiation is detected by photomultiplier tubes surrounding the detector.

In 1998, the Super-Kamiokande collaboration observed a clear deficit of atmospheric neutrinos coming from down side of the detector. This was the first indication for atmospheric neutrino oscillations. This observation is based on azimuthal angle dependence of the incoming neutrinos. Since atmospheric neutrino is isotropic, the number of neutrinos which are just produced above the detector and detected after a short distance, must be equal to the ones produced directly below to the earth and reach detector after traveling very long distance. The number of electron neutrinos coming from above and below are the same within error range. However, for muon neutrinos, it is not the case. The flux of muon neutrinos coming from below the detector is half of that coming from above. The detailed analysis showed that data is clearly explained by neutrino oscillation hypothesis [19].

2.4 Charmed Hadrons Production in Neutrino Interactions

In 1970, charm quark was proposed by S. Glashow, J. Illiopoulos and L. Maiani [20]. In 1974, charmonium which is a bound state of charm quark-antiquark pair called as J/ψ was discovered. It is a vector meson with a mass of 3.1 GeV^2 [21]. The study of neutrino induced charm production is important since the neutrino-nucleon interactions with opposite dimuon in the final state can be used to measure strange quark content of the nucleon and the value of the charm quark mass. Dimuon events in neutrino interactions were first observed in 1974 by HPWF collaboration at Fermilab [22]. In opposite-signed dimuon events, the leading muon

is interpreted as originating from the neutrino vertex and the other one is from decay of the charmed particle, as shown in Figure 2.5.

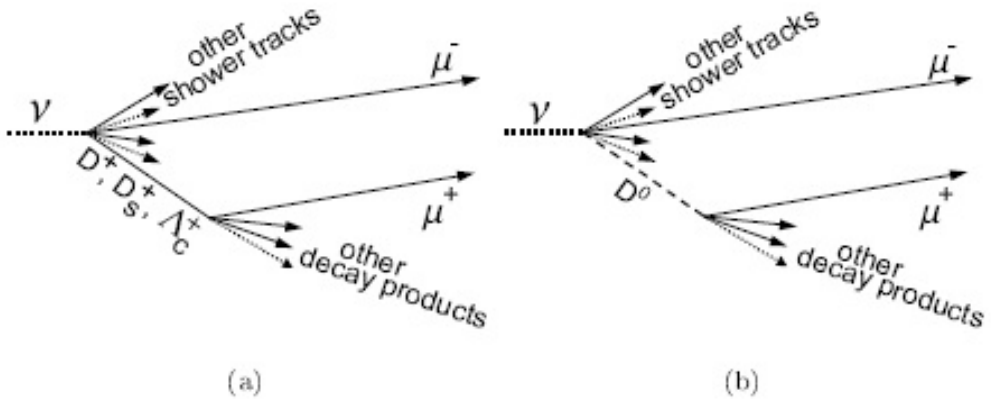

Figure 2.5: Production and decay of charmed hadrons in neutrino interactions.

The charmed hadrons can be produced in neutrino-nucleon interactions mainly through DIS and QE [23].

Deep inelastic charm production In DIS, a neutrino can produce a charm quark through CC interactions. However, charm cannot be detected itself only. The way to do is to dress up charm quark with anti-quarks for meson case, with two other quarks for baryon case [24]. Therefore fragmentation process plays an important role.

In the production of charmed hadrons, the neutrino DIS cross section for charm production can be written in terms of Bjorken x and y and structure function, $F_i^c(x, Q^2)(i \in 1, 2, 3)$ as

$$\frac{d^2\sigma(\nu_\mu N \to \mu^- cX)}{dxdy} = \frac{G_F^2 M E_\nu}{\pi(1 + Q^2/M_W^2)^2}[y^2 x F_1^c + (1 - y)F_2^c + (1 - \frac{y}{2})yxF_3^c], \tag{2.31}$$

where G_F is the Fermi constant, M_W is the mass of W boson. $F_i^c(x, Q^2)(i \in 1, 2, 3)$ are depend on Bjorken x and four-momentum transfer square Q^2. Eqn. 2.31 can be written as

$$\frac{d^2\sigma(\nu_\mu N \to \mu^- CX)}{dxdydz} = \frac{d^2\sigma(\nu_\mu N \to \mu^- cX)}{d\xi dy} \sum_h f_h D_c^h(z), \tag{2.32}$$

where

$$\xi = x(1 + \frac{m_c^2}{Q^2}). \tag{2.33}$$

Here m_c is the mass of charm quark. In Eqn.2.32, $D_c^h(z)$ stands for the probability distribution for the transformation of charm quark into charmed hadrons. The parameter z is the fraction of the charm quark energy carried by the charmed hadron and f_h is the average charmed hadron number [22].

Quasi-elastic charm production Quasi-elastic process occurs when a down valence quark turned into a charm quark. In other words, it is the transformation of target nucleon into a charmed baryon. The quasi-elastic reactions with charmed baryons in final state are

$$\nu_\mu + n \rightarrow \mu^- + \lambda_c^+, \tag{2.34}$$

$$\nu_\mu + n \rightarrow \mu^- + \Sigma_c^+, \tag{2.35}$$

$$\nu_\mu + n \rightarrow \mu^- + \Sigma_c^{*+}, \tag{2.36}$$

$$\nu_\mu + p \rightarrow \mu^- + \Sigma_c^{++}, \tag{2.37}$$

$$\nu_\mu + p \rightarrow \mu^- + \Sigma_c^{*++}. \tag{2.38}$$

The largest cross section contribution belongs to the process where λ_c^+ comes out. The contribution of other processes are very low. On the other hand, the ratio of quasi-elastic to total cross section is small at high energies. Therefore small number of λ_c^+ production is expected in the OPERA experiment since the average neutrino energy is 17 GeV.

2.5 Experimental Results on Charm Production in Neutrino Interactions

The charmed hadron production in neutrino interactions have been studied by several experiments like CDHS [25], CCFR [26], CHARM II [27], NOMAD [28], NuTeV [29] and CHORUS [30]. Among these experiments, E531 and CHORUS used nuclear emulsion technique. Both experiments took advantage of sub-miron resolution of nuclear emulsion to reconstruct the neutrino interaction vertex and charm decay vertex. In these experiments, the charged and neutral charmed hadrons are recognized on the basis of their decay topology. Therefore all

decay channels are studied in detail. The main disadvantage of nuclear emulsion experiments is the low statistics which was overcome in the CHORUS experiment by using massive target and automatic scanning systems.

In E531 experiment, the observed number of charm events is 122 out of 3855 located neutrino interaction events. The charm production rate relative to $\nu_\mu CC$ cross section is measured to be

$$\frac{\sigma_{Charmedhadrons}}{\sigma_{Total}} \simeq (5.4 \pm 0.7)\% \tag{2.39}$$

The breakdown of the observed topologies is given in the Table 2.2.

Table 2.2: The charm sample in the E531 experiment [30].

Charmed Hadron	Number
D^0	57
D^+	41
D_s^+	6
λ_c^+	14

In the CHORUS experiment the observed number of charm events is 2013 in 95000 $\nu_\mu CC$ events. The charm production rate relative to $\nu_\mu CC$ cross section is measured to be

$$\frac{\sigma_{Charmedhadrons}}{\sigma_{CC}} \simeq (5.9 \pm 0.4)\% \tag{2.40}$$

The breakdown of the observed topologies is given in the Table 2.3.

Table 2.3: The charm sample in the CHORUS experiment.

Charmed Hadron(s)	Topology	Number
D^0	V2	819
	V4	226
	V6	3
D^+, D_s^+, λ_c^+	C1	452
	C3	491
	C5	22

CHAPTER 3

THE OPERA DETECTOR

OPERA stands for Oscillation Project with Emulsion t-Racking Apparatus. The main goal of the OPERA experiment is to search for ν_τ appearance in almost pure ν_μ beam. The detector is located at Gran Sasso, 730 km away from the neutrino source, at CERN. It is a massive detector, containing 150,000 Emulsion Cloud Chamber so called (ECC), weight 1.25 kton. The construction and assembly of the OPERA detector took place between 2003 and 2008. Since then, data-taking has continued. In 2010, the first ν_τ interaction was detected by the OPERA collaboration [31].

3.1 The CNGS Beam

The OPERA neutrino beam is composed of almost pure ν_μ beam with a contamination of 2.1% $\overline{\nu}_\mu$ and 1% (ν_e and $\overline{\nu}_e$). The prompt ν_τ is estimated to be negligible. The average energy of the beam is 17 GeV [32]. The neutrino beam profile is shown in Figure 3.1.

Neutrino beam production at CERN begins in Super Proton Synchrotron (SPS) where protons are accelerated. At the end of SPS the beam is split into two parts one of them goes to Large Hadron Collider (LHC) and the second one goes to CNGS. When protons are reached 400 GeV/c momentum in SPS, they are directed to the carbon target. When protons hit the target, pions and kaons are produced. By means of horn and reflector, only positive charged pions and kaons are allowed to decay in the decay tube.

In Figure 3.2, main components are shown. The proton beam is coming from the left side. Target, horn, reflector and helium bag are located in the first 100 meters. It is followed by about 1000-meter long decay tube where pions and kaons are decay into μ^+ and ν_μ.

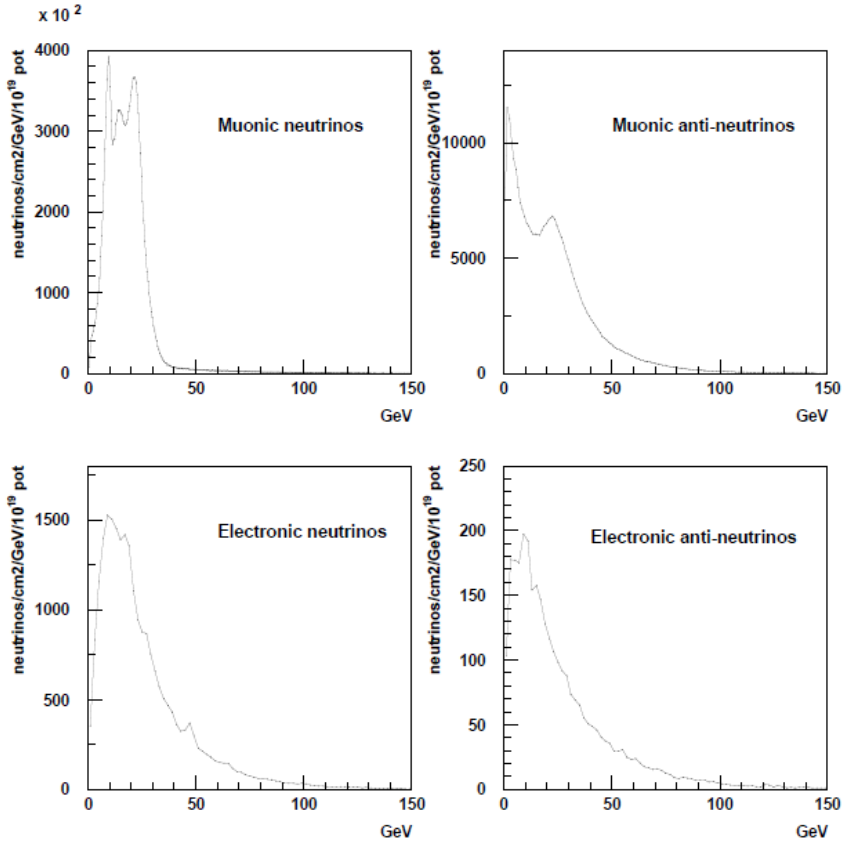

Figure 3.1: The four neutrino beam components of the CNGS [32].

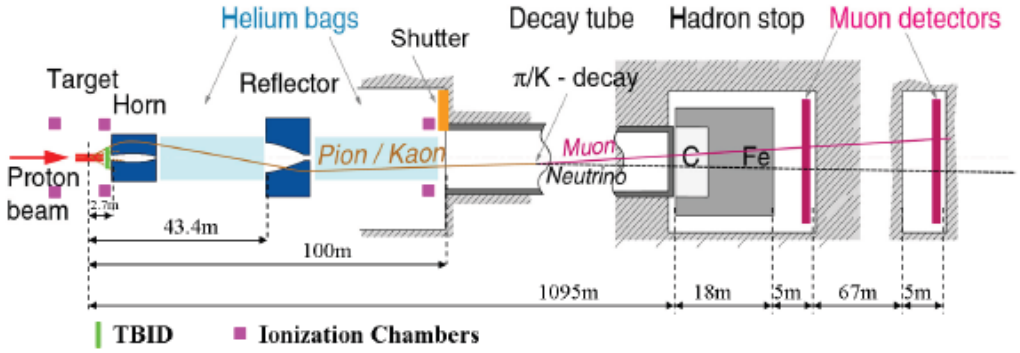

Figure 3.2: The CNGS Beam [32].

$$\pi^+ \longrightarrow \mu^+ + \nu_\mu \tag{3.1}$$

$$K^+ \longrightarrow \mu^+ + \nu_\mu \tag{3.2}$$

The hadron stopper, located at the end of decay tube, absorbs all hadrons as shown in Figure 3.2. These hadrons are, for example, protons which are not interacted in the carbon target or not decayed pions and kaons in the decay tube. On the other hand, muons can be absorbed as they travel through about half km of rock. Next to hadron stopper there are two muon detectors separated by 67 m. Muon detectors are used to measure neutrino beam intensity and to get information about beam characteristic [32]. Neutrino beam flux in terms of number of protons on target(pot) per year is given in Table 3.1.

Table 3.1: CNGS beam flux [33].

Year	Flux(pot)
2006	0.08×10^{19}
2007	0.08×10^{19}
2008	1.78×10^{19}
2009	3.52×10^{19}
2010	4.04×10^{19}
2011	4.79×10^{19}

3.2 The OPERA Detector

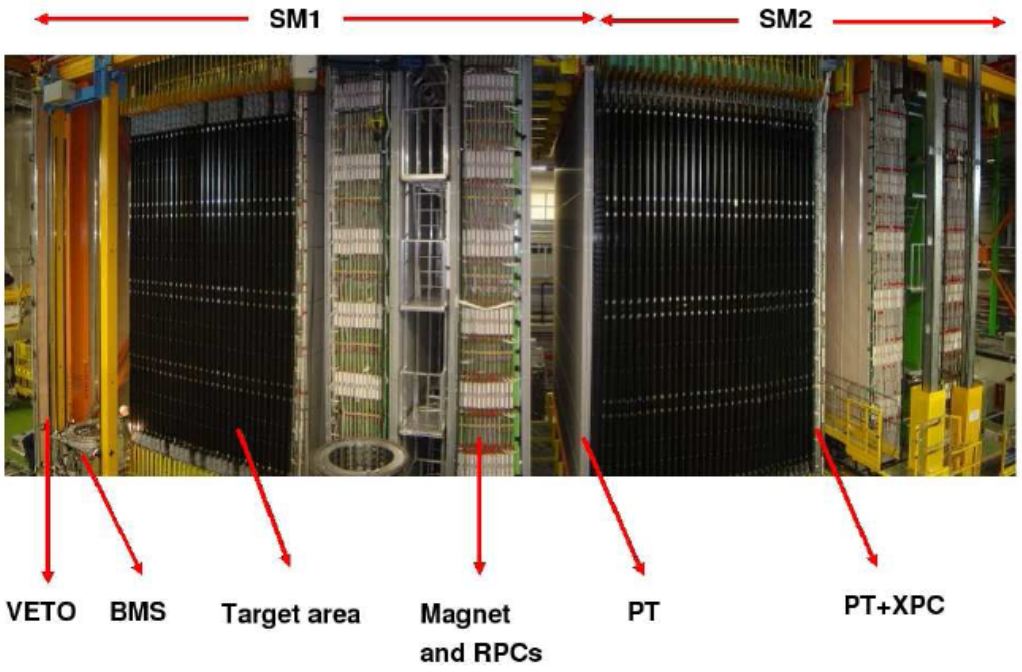

Figure 3.3: The OPERA Detector fish-eye side view [32].

The OPERA detector shown in Figure 3.3 is placed in the Hall C of LNGS. The OPERA detector is made of two identical super modules (SM1 and SM2). Each consists of target area and spectrometer. The target area is made of walls, filled with bricks, and double layer of plastic scintillator or target trackers (TT) are attached next to the walls. There are 31 walls, capable of hosting 2912 bricks, is made of light stainless steel. The number and weight of the bricks are huge, therefore bricks are produced by a machine called Brick Assembly Machine (BAM) and for installation Brick Manipulator System (BMS) is used. Next to target area, muon spectrometer is placed. Magnetic spectrometers consist of iron magnet, Resistive Plate Chambers(RPC), drift tubes. Before the SM1, a structure called VETO take place. Its aim is to reject charged particles coming from surrounding. Each sub-detectors and its characteristics will be explained in detail in the next section.

3.2.1 The OPERA Bricks

The main component of the OPERA experiment is ECC brick since it acts as target and detector for neutrino interactions. The OPERA bricks have a sandwich structure. It is composed of 57 nuclear emulsion films and 56 lead plates, shown in Figure 3.4. The lead plates are 1 mm thick.

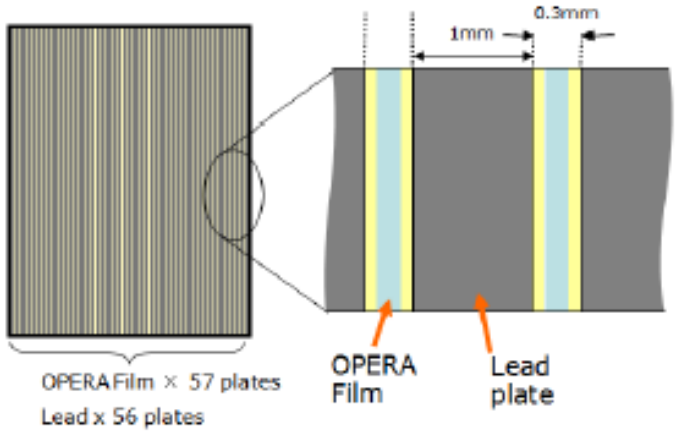

Figure 3.4: Schematic view of an ECC brick in the target wall [32].

The lead plates, have high density and short radiation length, are chosen as a passive material for neutrino interactions. High density enhances the neutrino interaction rate. Short radiation

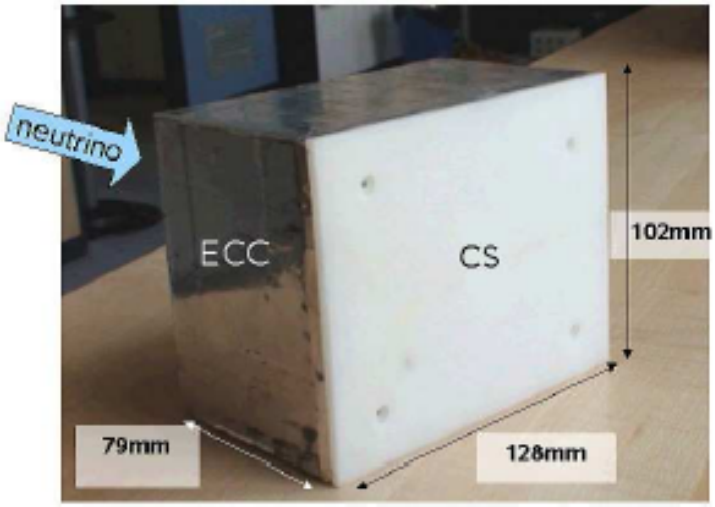

Figure 3.5: The OPERA Brick with Changeable Sheets attached [32].

length is good for momentum measurement through multiple scattering. On the other hand, lead is a radioactive thus it can cause background tracks. However by choosing less radioactive lead, this effect may be ignored. Another possibility for plates was iron because its price is low, not radioactive and has better mechanical properties than lead. However due to its low density, 30% of more emulsions have to be used to have same number of neutrino interactions in the target. It makes iron globally more expensive. Thus lead is chosen as a passive material [34].

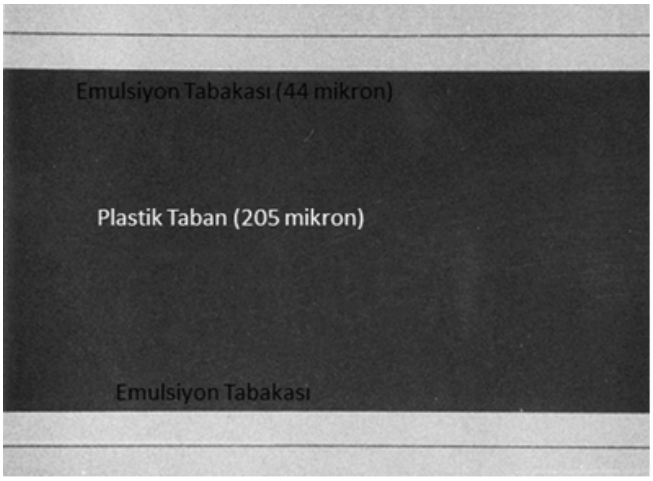

Figure 3.6: The OPERA Changeable Sheet.

On the other hand nuclear emulsions act as tracking detector with sub-micron spatial resolution for charged particle. The OPERA emulsion films consist of two a 44-micron thick nuclear emulsion layers in both sides of a 205-micron thick plastic base as shown in Figure 3.6. The film production had been done by FuJi Film company between 2003 and 2005.

Nuclear emulsions films are composed of AgBr crystals with a gelatin layer. When a charged particle passes through nuclear emulsion, Ag ions, so called latent images, are formed. After a chemical process, called as development, this image becomes visible under the optic microscope. Therefore, three dimensional trajectory of charged particles can be reconstructed. Then, charged particles trajectory can be seen. These developed films must be kept about 20 C° temperature and 60% relative humidity.

The OPERA bricks were designed in order to minimize the amount of passive material around the bricks. The dimensions of the OPERA bricks are 79 mm in the longitudinal and 128 mm $\times$ 102 mm in transverse plane as shown in Figure 3.5. Although bricks are small in size, their weights are 8.3 kg. At the surface of each brick two Changeable Sheets (CS) are attached as shown in Figure 3.7. They are used to verify the information coming from the electronic detectors. After finding the right brick, what to be checked first is to understand whether there is a relevant interaction occurred in the brick or not, that is why CS's are first to be scanned. After finding the predicted tracks in the CS's, the 57 emulsion plates in the corresponding brick are scanned in order to locate the neutrino interaction.

3.2.2 The Target Trackers

In the target area there are 62 walls, each is interleaved with two target tracker (TT) planes as shown in Figure 3.8. Each TT plane is made of 4 horizontal and 4 vertical modules that have scintillation with 6.86 m long, 26.3 mm wide and 10.6 mm thick. For read out, 64 Wavelength Shifting (WLS), connected to multi-anode photo multipliers (PMT) as shown in Figure 3.9. Target trackers cover the area of $6.7 \times 6.7\ m^2$. They provide real time tracking of the charged particles. The main task of the target tracker is to locate the brick where neutrino interaction has occurred. The brick wall and TT are placed very close to each other in order to have a good spatial resolution.

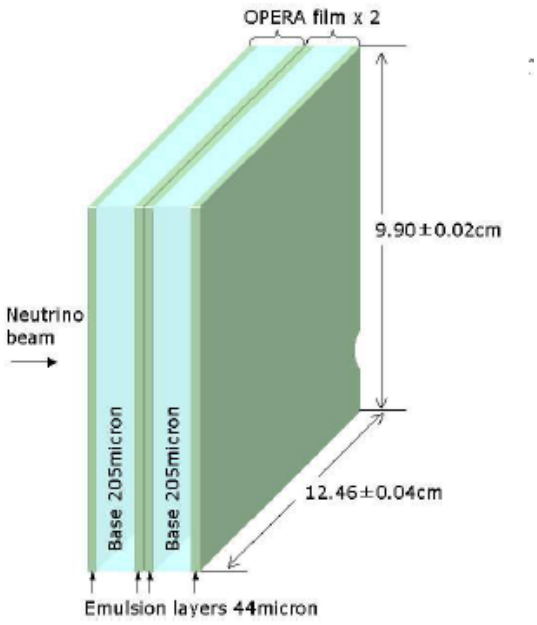

Figure 3.7: CS doublet [32].

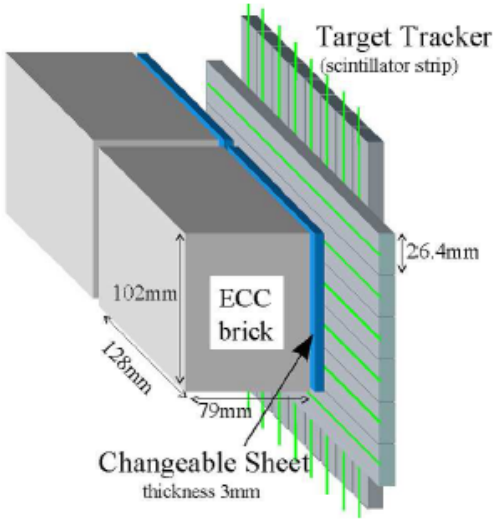

Figure 3.8: Schematic view of target trackers located very close to the wall [32].

3.2.3 The Magnetic Spectrometers

There is magnetic spectrometer at the end of each super module. The main task of the muon spectrometer is to measure the muon momentum and its charge. The classification of neutrino

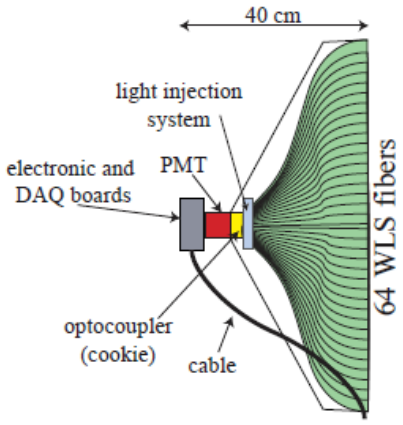

Figure 3.9: Schematic view of a scintillator strip end-cap [32].

events are done according to the information coming from the spectrometers.

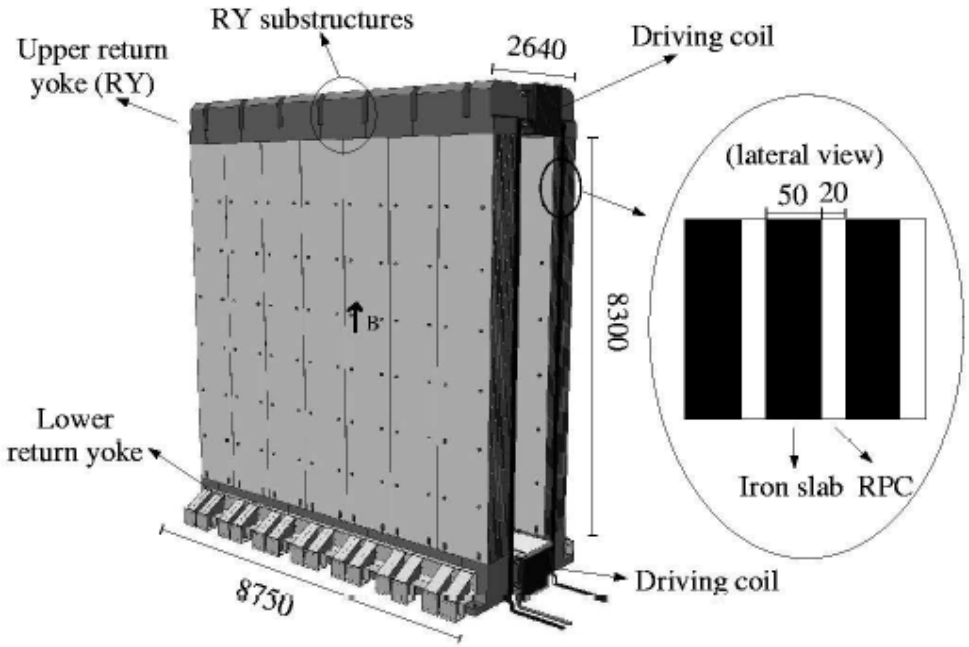

Figure 3.10: The schematic view of the OPERA magnet [32].

The OPERA muon spectrometers consist of electronic RPC (Inner Tracker), drift tubes and magnet. The magnet is oriented transverse to the neutrino beam axis, in Figure 3.10, and its sizes are about 10 meter long 8.75 m wide and has a depth of 2.64 m. The average measured

magnetic field is approximately 1.53 Tesla where the operated current is 1600 Amper in the normal conditions. Each OPERA magnet is made of two vertical walls connected with flux return yokes at top and bottom. Walls are built by combining twelve iron layers consisting of 50 mm thick iron slabs. RPC's are located between each layer as shown in Figure 3.10. Their function is to reconstruct muon tracks inside spectrometers.

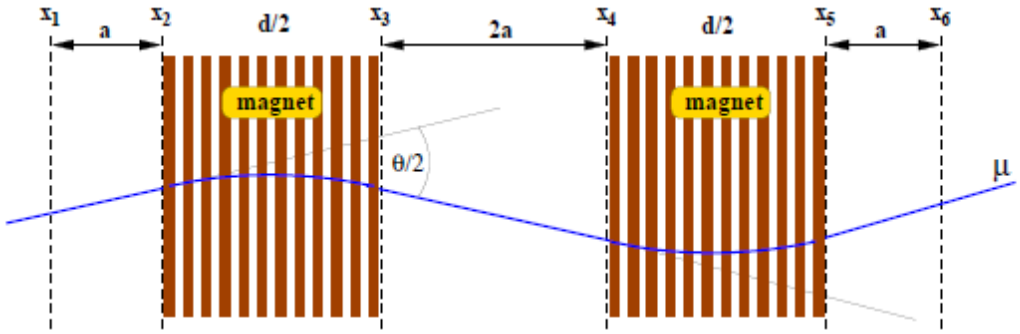

Figure 3.11: The deflection of the muon in the magnetic field [32].

The RPC system is separated into two sub-detectors, called the Inner Tracker and XPC. The Inner Tracker(IT) is the tracking system inside magnets. There are 22 RPC planes in IT. Each IT plane consists of RPC planes which are divided into 3 columns and 7 rows. Thus in total $22 \times 3 \times 7 = 462$ RPC's are located in the detector. It is impossible to replace the RPC after installation due to the magnet design. Therefore it is handled very carefully and tested many times for different aspects. The average tracking efficiency is measured as 98%. The XPC are two RPC planes, rotated ±42.6° with respect to horizontal, located in the upstream of the magnet. They are outside of the iron magnet, placed next to upstream of first drift tube system and downstream of second drift tube system. Each XPC plane is made of 21 RPC consisting of 7 rows differs in size for first and second planes.

The Precision Tracker(PT) is a part of the muon spectrometer as shown in Figure 3.12. Its task is to identify muon and measure its charge and momentum. When muons pass through the magnets, they are deflected in opposite direction and moving in the horizontal plane due to the opposite magnetic field in magnets as shown in Figure 3.11. The drift tubes gas is a mixture of 80% Argon and 20% CO_2. The pressure is kept at absolute pressure, 1005±5 mbar, in order to have a uniform gas density [32]. Intrinsic resolution of PT is 0.3 mm, however an overall resolution is 0.5 mm. Momentum resolution $\Delta p/p$ is expected to be better than 30%. In addition to PT's, Inner trackers provide a measurement of the range of muon's which stop

Figure 3.12: Drift tubes [32].

in the iron. Thus in total the spectrometers provide the measurements needed to study the muonic τ decay channel [35].

3.2.4 The OPERA Physics Performance

In the OPERA experiment, the neutrino beam consists of almost pure muon neutrinos. Therefore on the target, it is expected to have mainly muon neutrino interactions.

Depending on the neutrino flavour, CC neutrino interaction in the OPERA target produce muon or tau lepton in addition to hadrons. In the of case of NC interaction only hadrons are produced as charged particles. Therefore it is harder to locate NC neutrino interactions in the OPERA brick.

3.2.5 Oscillation Analysis Steps

In order to detect ν_τ appearance, τ production and decay vertices must be located in the brick. The decay channels of τ^- lepton studied in the OPERA experiment are

$$\tau^- \longrightarrow e^- + \overline{\nu}_e + \nu_\tau, \tag{3.3}$$

$$\tau^- \longrightarrow \mu^- + \overline{\nu}_\mu + \nu_\tau, \tag{3.4}$$

$$\tau^- \longrightarrow X + \nu_\tau, \tag{3.5}$$

where X corresponds to all hadrons which are mainly pions. These decay channels are called electronic, muonic and hadronic. The ECC detector is very convenient to identify electron by locating its shower. Thus, this allows the study of electron channel with a high efficiency. For muon channel, a cut is applied on the muon momentum in order to suppress the background. The muon momentum should be between 1 GeV and 15 GeV. Hadronic channel which has the largest branching ratio is difficult to study due to high background. The kinematic cuts must be applied in order to reduce background [35]. The main background to the oscillation signal is the charmed hadron. If the primary muon in $\nu_\mu CC - Charm$ events is not identified, charm decay mimics the tau decay. The charm background estimated using MC simulation is less than 1. The charm events are categorized as short and long according to vertex position. If the neutrino interaction vertex and τ decay vertex are in the same lead plate. This decay topology is called short. If neutrino interaction vertex and decay vertex are found in different plates, it is named as long.

After a neutrino interaction is triggered, the Target Trackers detect the position of the brick where the neutrino interaction occurred. Brick Manipulator System (BMS) extracts the corresponding brick from the target wall. Then, the corresponding brick is marked with X ray in order to determine alignment of two Changeable Sheets (CS). The two CS's are removed from the box and taken to the development facility. After the development process, emulsion films are scanned using full automatic microscope systems located in Gran Sasso and Japan. If the predicted tracks are found in the CS's. The corresponding brick exposed to X ray for the lateral mark. After that the bricks are exposed to the cosmic rays to have better alignment of emulsion films. Then, emulsion films are developed and sent to the scanning laboratories in JAPAN and Europe including Ankara. The automatic microscope in Ankara is shown in Figure 3.13.

3.2.6 Automatic Scanning System and Emulsion Scanning

There are two types of full automatic microscope systems, called as SUTS and ESS. SUTS stands for Super Ultra Track Selector, used in Japan. ESS stands for European Scanning System, pioneered by Salerno group in the OPERA collaboration.

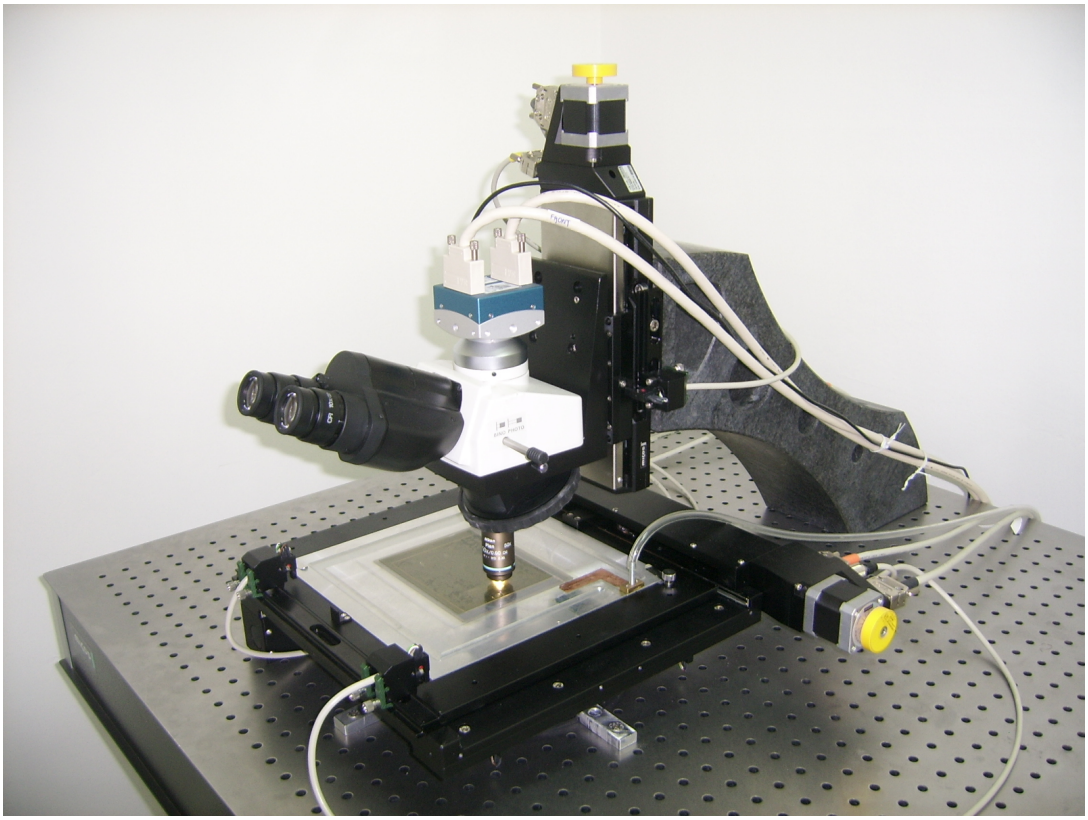

Figure 3.13: The ESS microscope in METU [32].

The automatic microscope consists of a massive MICOS table, CMOS camera which can move (vertically) Z direction and a stage can move in both X and Y directions. Under the scanning table illumination system is located as shown in Figure 3.14.

During the emulsion scanning, the stage moves horizontally and CCD camera moves vertically to take tomographic images of emulsion at different layers. The motion of the horizontal stage (maximum speed, acceleration, deceleration, ...) was set in order to minimize the scanning time. On the other hand, during data taking, the vertical stage moves at constant speed calculated by taking into account the camera frame rate, the number of desired frames and the emulsion thickness 44 mm. The time for a cycle is thus obtained by adding the time for horizontal displacement, the time that the vertical stage takes to reach its starting position and the time needed for the data acquisition in Z. In total, ESS speed is approximately 20 cm^2/h in an emulsion volume of 44 mm thickness [36].

After taking the images, they are processed by a digital filter to enhance the contrasts between pixels. A threshold is applied to the selected pixels which become grain later. A grain is

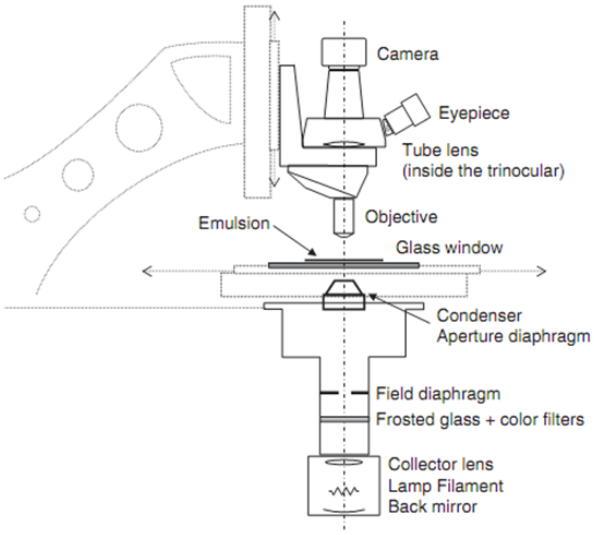

Figure 3.14: Schematic layout of the ESS microscope optical system [32].

defined as a cluster of about 15 pixels. If there is a sequence of aligned grains in an emulsion layer, it is defined as the micro track. If the angles of micro tracks beyond the plastic base are in a good agreement, they form the base track as shown in Figure 3.15. By connecting these base tracks plate by plate trajectories of charged particles can be reconstructed [37].

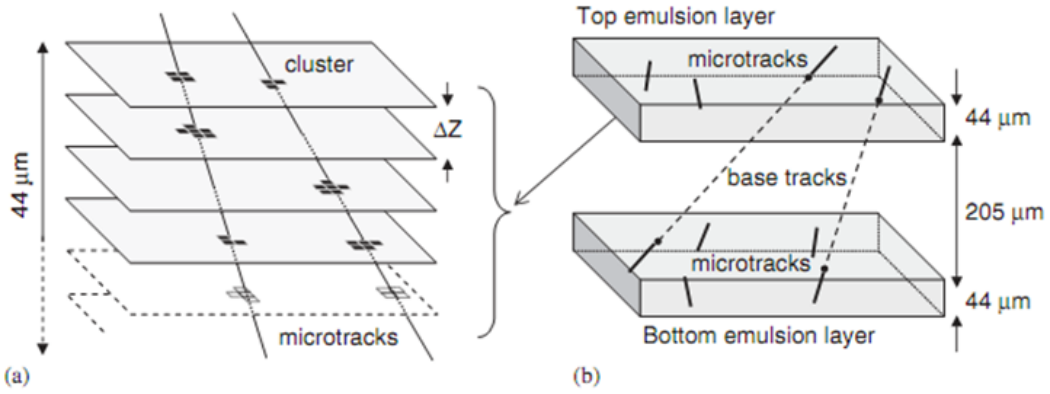

Figure 3.15: (a)Micro track reconstruction in one emulsion layer by combining clusters belonging to images at different levels,(b)micro track connections across the plastic base to form base tracks [32].

If the base track in the most upstream plate is found, then searched for in the next plate, and then followed upstream in each consecutive plate. In each emulsion plate, the track segments are followed. Until they disappear in 3 consecutive plates. This scanning is called scan-back. The first plate where segment disappears is called as vertex plate [38].

There are three possible reasons to miss the scan-back track in the scanning procedure.

Primary vertex The scan-back track may originate from a neutrino vertex where it is the most upstream plate.

Secondary vertex The scan-back track may originate from a secondary vertex where the primary vertex is further upstream.

Inefficiency It may be resulted from scanning inefficiency, miss alignment of emulsions and wrong measurement of the track.

For each event, these three cases are investigated. This procedure is called as vertex search [14]. The reconstruction algorithm performance and reconstruction efficiency estimation are the subject of next chapter.

CHAPTER 4

DATA ANALYSIS

The OPERA analysis software framework, OpRelease [39] is written in C++ and used for Monte Carlo (MC) production and data/MC reconstruction. The OpRelease framework is the combination of followings: data model, detector simulation, physics simulation and event reconstruction and analysis [40]. It is composed of a group of package which are governed by CMT(Configuration Management Tool) [41]. CMT requires some external softwares like CERNLIB [42], CLHEP [43], ROOT [44], Pythia6 [45] that is need by ROOT, ROOT Virtual Monte Carlo and ORACLE [46] for library and Data Base access. Data are stored in root files with a directory structure [47]. The tree structure of OpRelease is shown in Table 4.1.

Table 4.1: OpRelease tree structure [48].

TTree name	OpRData Clasess	Operation
TreeRD	REMULZone.h REMULView.h REMULRawData.h	Volume Scan
TreeAL	REMULLayerAlignment.h	Allignment
TreeTK	REMULTrack.h REMULTrackKinematic.h	Tracks reconstruction
TreeVX	REMULVertex.h	Vertex reconstruction
TreeDataMap	REMULDataMap.h	Data set description & logical relations
TreePredTT	REMULPredTT.h	Electronic detectors prediction
TreeCSAndScan	REMULCSAndScan.h	CS, Scan Back, Scan Forth
TreeManualCheck	REMULManualCheck.h	Manual chacks
TreeMCR TreeRealReco	Rparticle.h, Rvertex.h, REMULDigit.h, REMULHit.h, ...	MC & electronic detector data

The data model implemented in OpRelease is given in Figure 4.1.

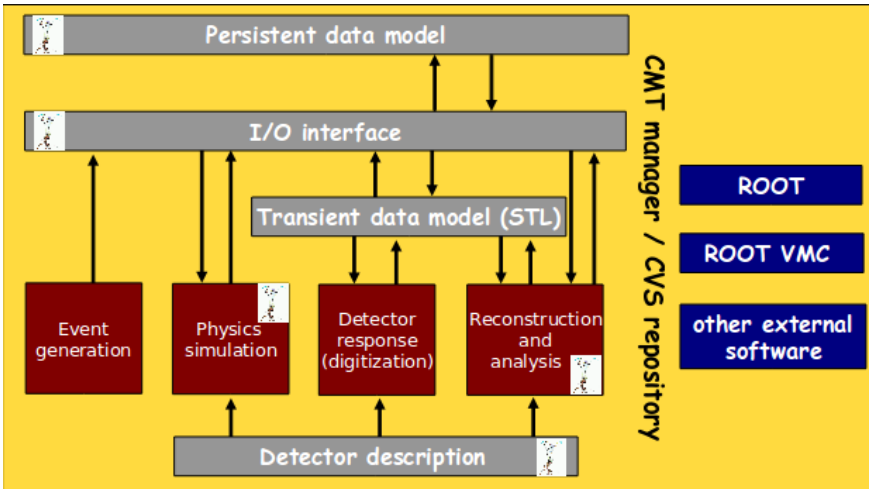

Figure 4.1: The Data Model [40].

As an event generator OpNGEN is used. It produces ascii files with four-vector information of the event which are then transformed into root files by using a root macro. The output of OpNGEN is used as an input to OpEmuIo which produces root files based on implemented emulsion data model. The output root file contains zone, view and raw data information. This output files are given as input to OpEmuRec which performs the event reconstruction. One can perform event reconstruction with two different reconstruction algorithms so called Fedra [49] and SySal [50]. In this analysis SySal has been used for the event reconstruction. In addition to the OPERA analysis package an analysis code has been developed for this thesis work.

The offline reconstruction of Data and MC events follows several steps. The first step is the reconstruction of the micro-tracks which are aligned grains found at different levels of the emulsion layer. Then, micro-tracks found at each layer of emulsion films are connected through the plastic base to form so called base-tracks. In order to define a reference frame for the track reconstruction, affine transformations including shifts, rotation and expansion in consecutive emulsion plates are performed using cosmic tracks present in the brick. Then, in order to reconstruct the charged particle tracks, base tracks are connected plate by plate. This reconstruction is performed by Kalman filter algorithm. After the track reconstruction, vertex search has been done using the minimum distance search between the reconstructed tracks. The final vertex finding and fitting are again performed by Kalman filter algorithm. In order to reconstruct one vertex at least two tracks must be reconstructed in the event.

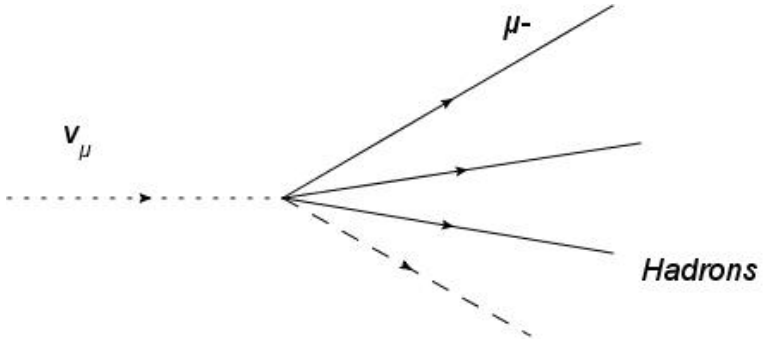

Figure 4.2: Neutrino CC interaction with only one vertex.

In the OPERA experiment, the neutrino interaction in the brick is called primary vertex. In Figure 4.2, ν_μ CC interaction with μ^- and charged hadrons is shown. The most of the ν_μ CC events contain only primary vertex. But if a charmed hadron is produced and it decays in the brick, a secondary vertex is identified in addition to the primary vertex as shown in Figure 4.3. The fraction of this topology is only few percent.

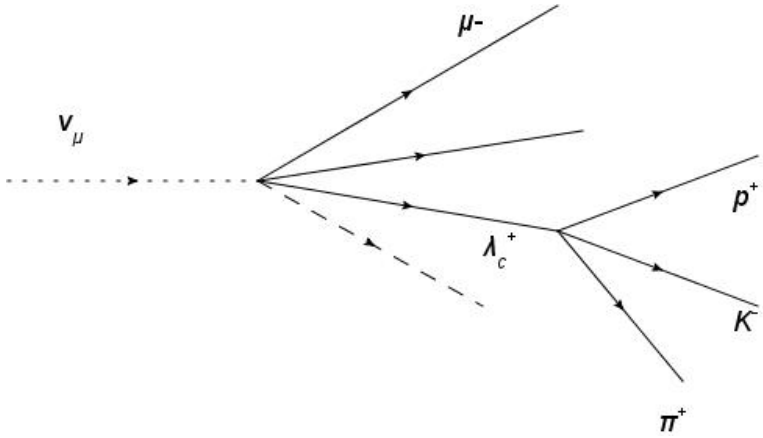

Figure 4.3: Neutrino CC interaction with more than one vertex.

4.1 Reconstruction Efficiency

In order to estimate vertex reconstruction efficiency, 3000 $\nu_\mu CC$ and 3000 $\nu_\mu CC - Charm$ Monte Carlo events, generated with OpNGen and reconstructed with SYSAL algorithm are used. $\nu_\mu CC$ events contain 92% DIS and 8% QE interactions. After analyzing MC events using our analysis code, we obtain vertex reconstruction and muon reconstruction efficiency.

The mean number of reconstructed vertex in $\nu_\mu CC$ is 1.27 as shown in Figure 4.4. It is higher than 1 since the reconstruction algorithm can reconstruct also photon conversion and secondary interactions.

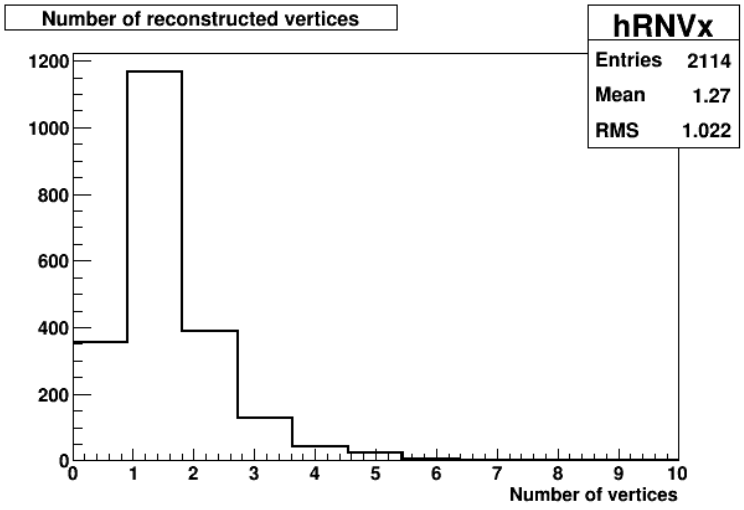

Figure 4.4: Number of reconstructed vertices.

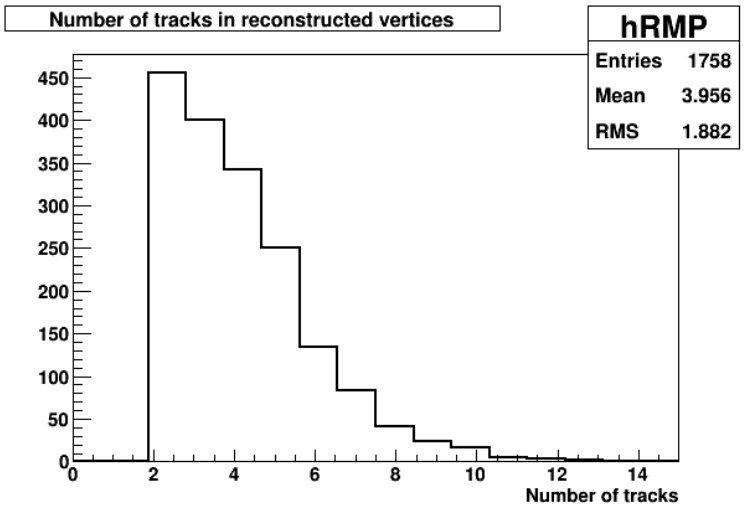

Figure 4.5: Number of reconstructed tracks at the primary vertex.

On the other hand, there is 17% of events with zero reconstructed vertex. These events are mainly quasi-elastic containing only reconstructed muon track. In 55% events only one vertex is reconstructed. The remaining fraction (28%) of events contains more than one reconstructed vertex. In this multi vertex events, the vertex is defined as primary if the muon track is attached to it. There are 1560 events with muon track attached to the primary vertex. In case,

Table 4.2: The breakdown of reconstructed MC events.

Event sample	$\nu_\mu CC$	$\nu_\mu CC - Charm$
Total number of events	3000	3000
Non-empty events	2114	2193
Events with at least one rec. vertex	1758	2024
Events with zero rec. vertex	355	170

the muon track is not reconstructed, vertex with highest multiplicity is selected as a primary vertex. There are 1758 events with one reconstructed primary vertex. The mean number of reconstructed primary tracks is 3.95. Figure 4.6 shows the impact parameter distribution of primary tracks to the vertex position. The mean value of impact parameter of primary tracks is 2.8 μm [51].

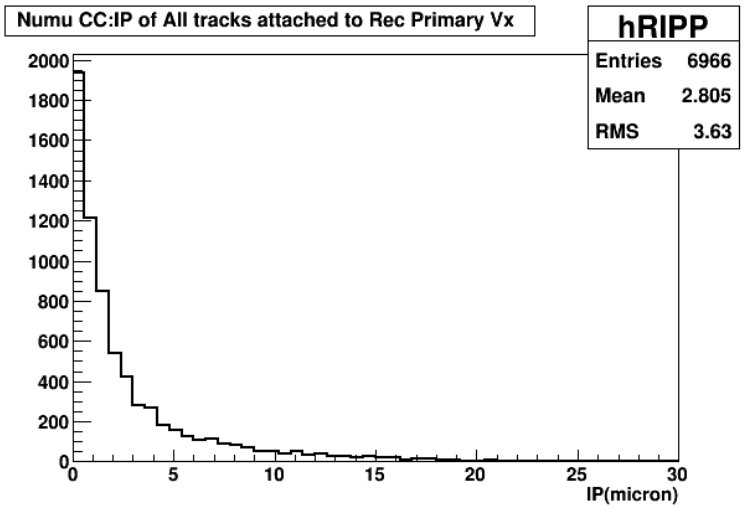

Figure 4.6: IP distribution

Figure 4.7, 4.8 and 4.9 show the difference between true and reconstructed vertex positions along x, y, and z axis respectively. The long tail in the distribution is due to wrong reconstruction of the primary vertex. The fraction of $\nu_\mu CC - Charm$ events with a reconstructed primary vertex is 90.2%

In order to compare event reconstruction efficiency in $\nu_\mu CC$ and $\nu_\mu CC-Charm$ MC events, the same analysis is done using the charm events. In $\nu_\mu CC - Charm$ sample, the mean number of reconstructed vertex is 1.5 which is higher than for $\nu_\mu CC$ events due to charm production and decay. The charm decay vertex can be reconstructed if the decay is multi-prong. The single

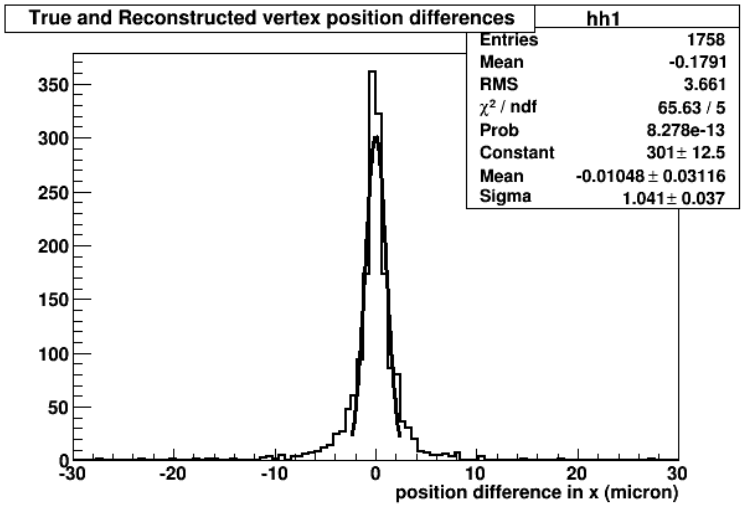

Figure 4.7: The difference between true and reconstructed vertex position in x.

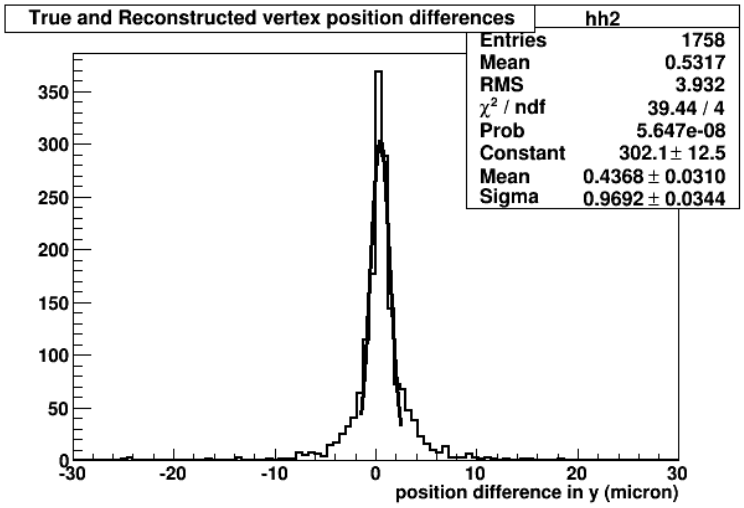

Figure 4.8: The difference between true and reconstructed vertex position in y.

prong decay can be reconstructed if the decay is long one and parent particle is reconstructed. The selection of primary vertex is the as same as $\nu_\mu CC$ events selection. In the selection of secondary vertex, the true daughter track information is used. The tracks in the secondary vertex are compared with true charm daughter tracks. If the reconstructed tracks match with the true daughter tracks, the corresponding vertex is tagged as a real secondary vertex.

Figure 4.10 shows the impact parameter distribution of primary tracks to the vertex position in $\nu_\mu CC - Charm$ events. The mean value of impact parameter of primary tracks is 3.9 μm. It is about 1.1 μm larger than one for $\nu_\mu CC$ events. It is due to migration of tracks which will

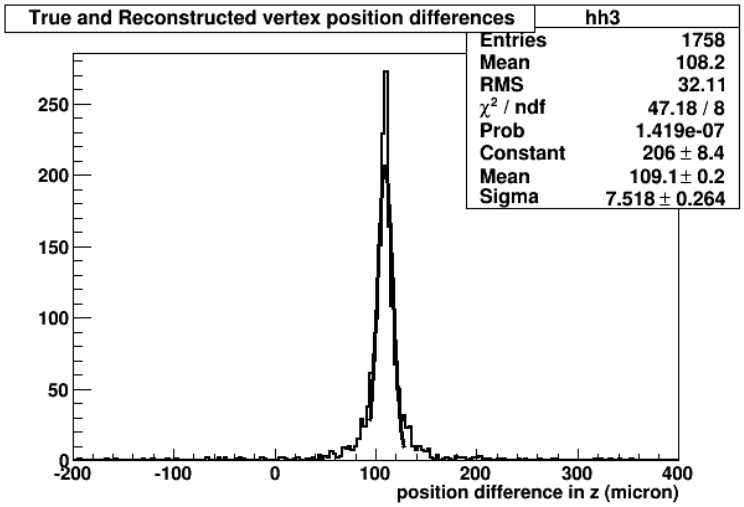

Figure 4.9: The difference between true and reconstructed vertex position in z.

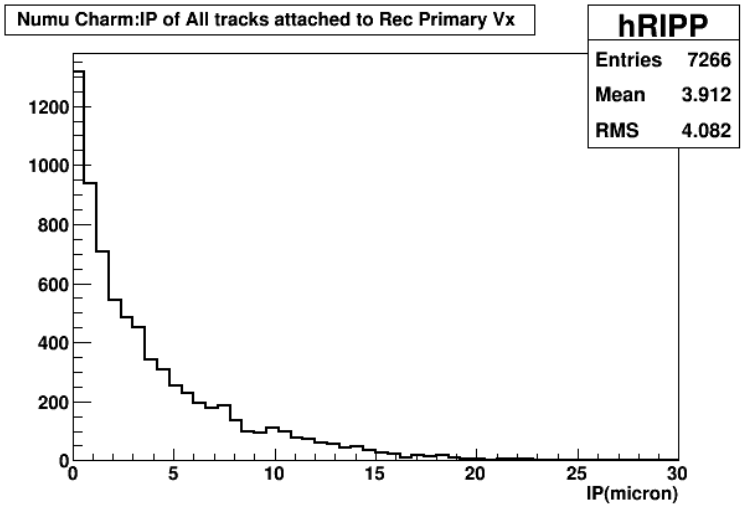

Figure 4.10: IP distribution for $\nu_\mu CC - Charm$.

be explained in the last section.

Figures 4.11, 4.12 and 4.13 show difference between true and reconstructed primary vertex positions along x, y, and z axis respectively. The tail in the distribution is due to wrong reconstruction of the vertex. It is found that the primary vertex is reconstructed with a resolution of 10 μm in x and y positions. But there is a systematic shift of 86 μm in z position. Using the reconstructed primary and secondary vertex positions, flight length of the charmed hadrons can be estimated.

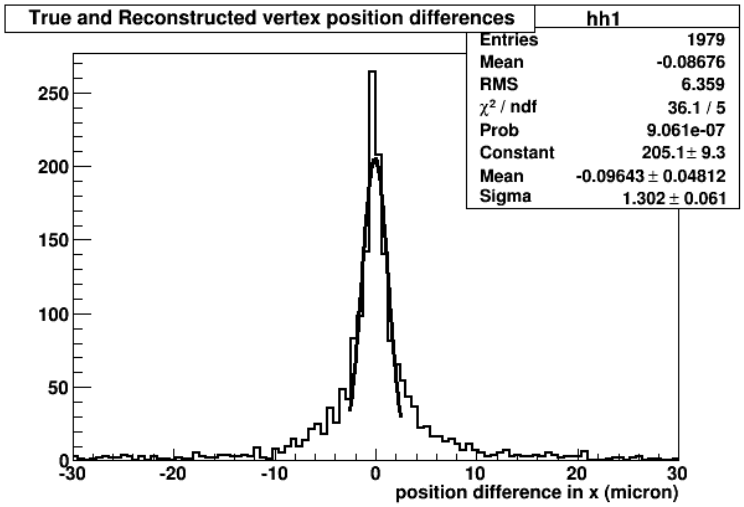

Figure 4.11: The difference between true and reconstructed vertex position in x for $\nu_\mu CC - Charm$.

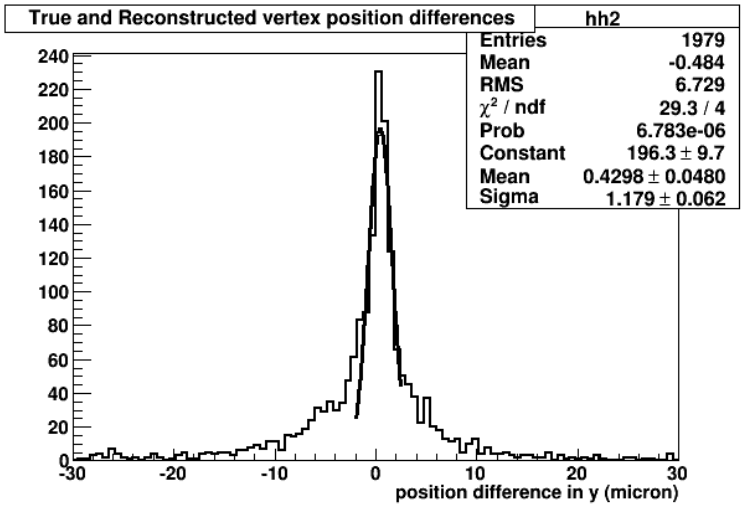

Figure 4.12: The difference between true and reconstructed vertex position in y for $\nu_\mu CC - Charm$.

As seen in Figure 4.14 and 4.15, there is a reasonable agreement between true and reconstructed flight lengths.

The secondary vertex reconstruction efficiency is shown in Figure 4.16. In short decay topologies (Flight length between 0 and 1300 μm), the reconstruction efficiency of secondary vertex is low so is flight length. Since the true primary and secondary vertices are clustered as a single vertex, which is tagged as the primary vertex by the reconstruction algorithm. In general the efficiency increase with the flight length.

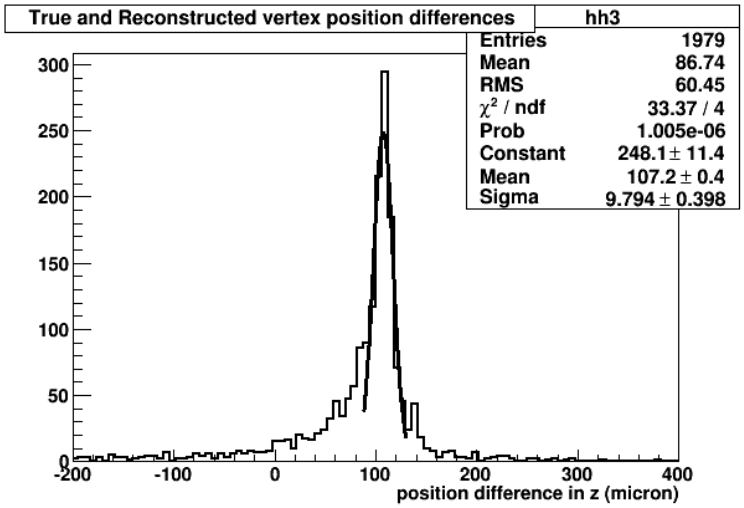

Figure 4.13: The difference between true (histogram) and reconstructed (crosses) vertex position in z for $\nu_\mu CC - Charm$.

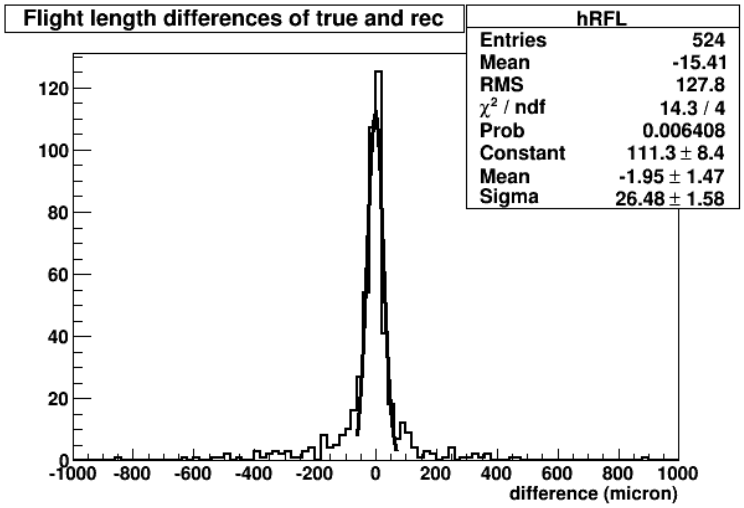

Figure 4.14: The difference between true and reconstructed flight length of charmed hadrons.

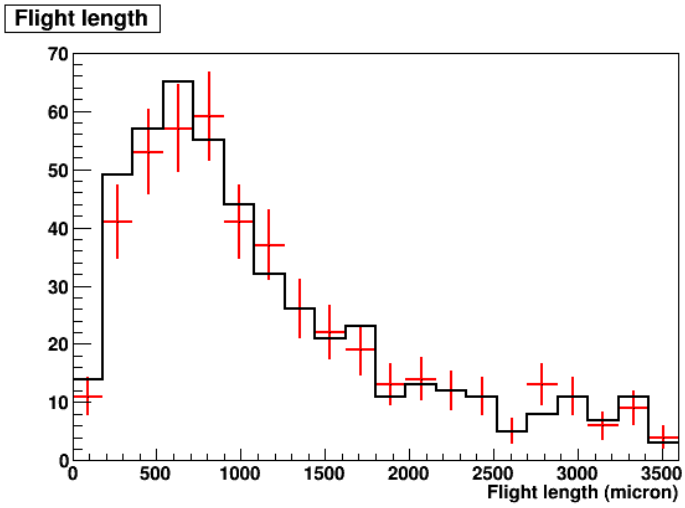

Figure 4.15: The true (histogram) and reconstructed (cross marks) flight length distribution of charmed hadrons.

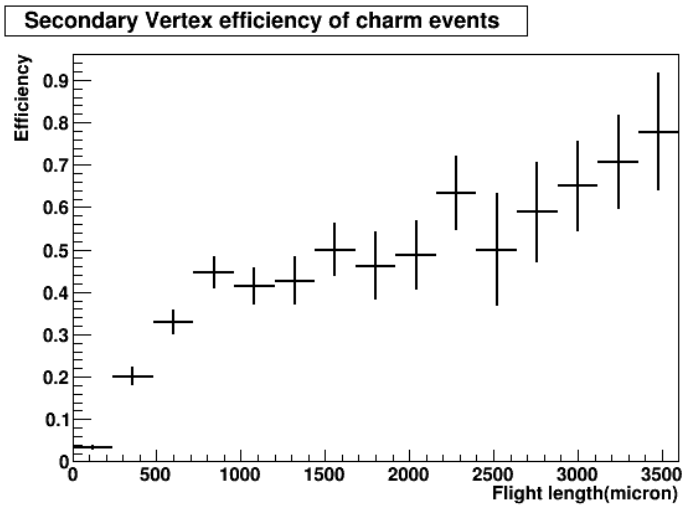

Figure 4.16: Secondary vertex reconstruction efficiency as a function of flight length.

4.2 The Muon Reconstruction Efficiency

The muon reconstruction efficiency as a function of muon momentum and slope has been evaluated for $\nu_\mu CC$ and $\nu_\mu CC - Charm$ events. Figure 4.17 shows the muon reconstruction efficiency as a function of muon momentum. The efficiency is flat at about 80% up to 15 GeV momentum then it decreases slowly.

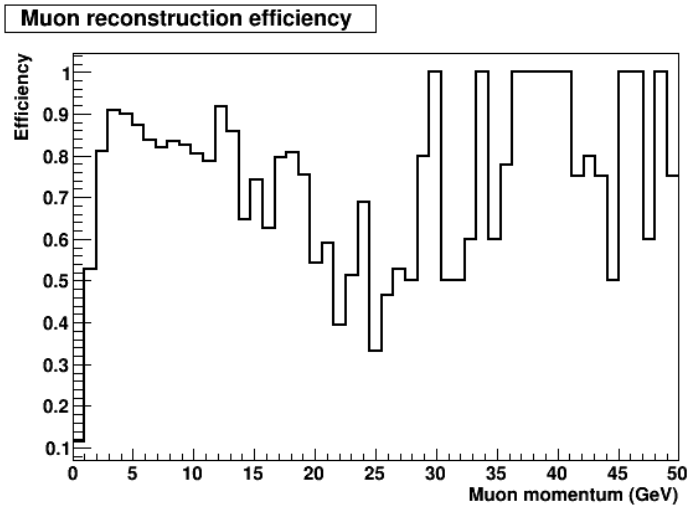

Figure 4.17: Muon reconstruction efficiency vs muon momentum.

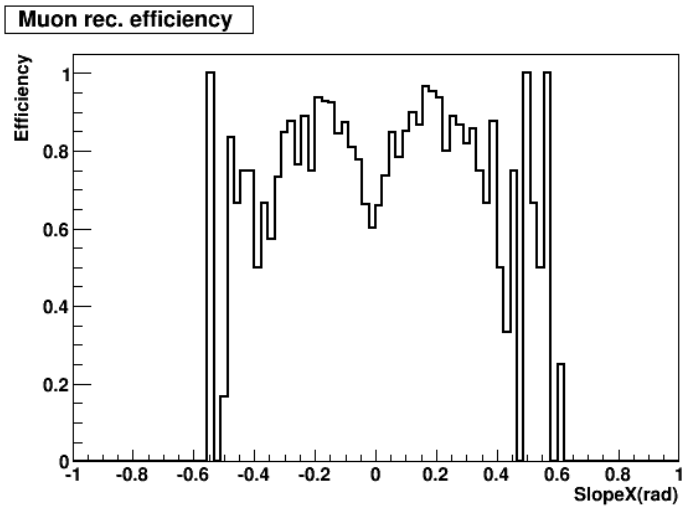

Figure 4.18: Muon reconstruction efficiency vs x slope.

Figure 4.18, 4.19 shows efficiency as function of muon slope. The efficiency drops gradually around 0 rad. This drop is investigated in detail. The main reason for the inefficiency is

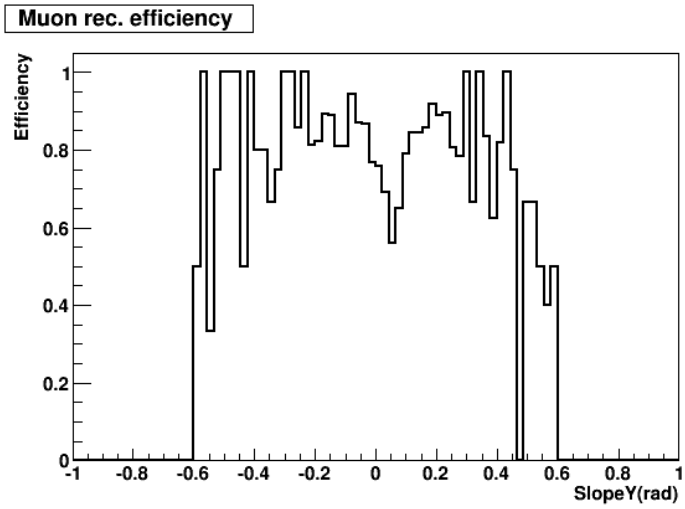

Figure 4.19: Muon reconstruction efficiency vs y slope.

QE-like topologies in which only muon track is reconstructed but not the primary vertex. This causes a sharp drop in efficiency in the region of -0.1 and 0.1 rad. On the other hand, Figure 4.20 shows the muon reconstruction efficiency as a function of muon momentum. The efficiency is flat at about 80% after 4 GeV momentum. Similarly, Figures 4.21 and 4.22 show the efficiency plotted as a function of muon angle for $\nu_\mu CC - Charm$ events. The efficiency is flat at about 80%. This can be explained by the fact that $\nu_\mu CC - Charm$ sample contains only DIS events which have more than one reconstructed track.

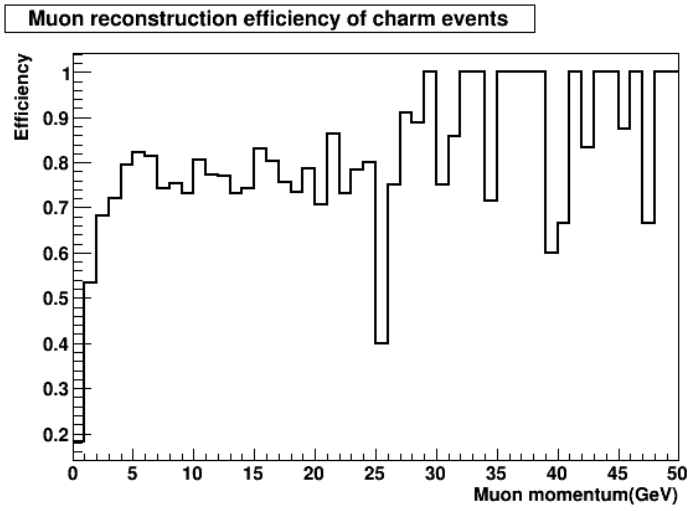

Figure 4.20: Muon reconstruction efficiency vs muon momentum for $\nu_\mu CC - Charm$.

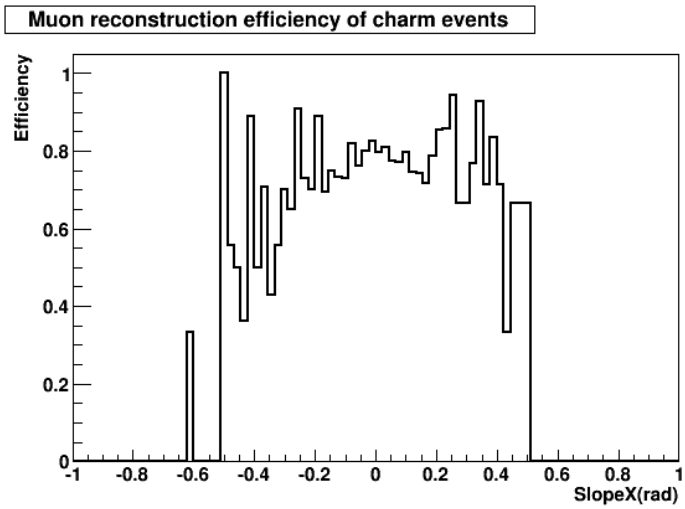

Figure 4.21: Muon reconstruction efficiency vs x slope for $\nu_\mu CC - Charm$.

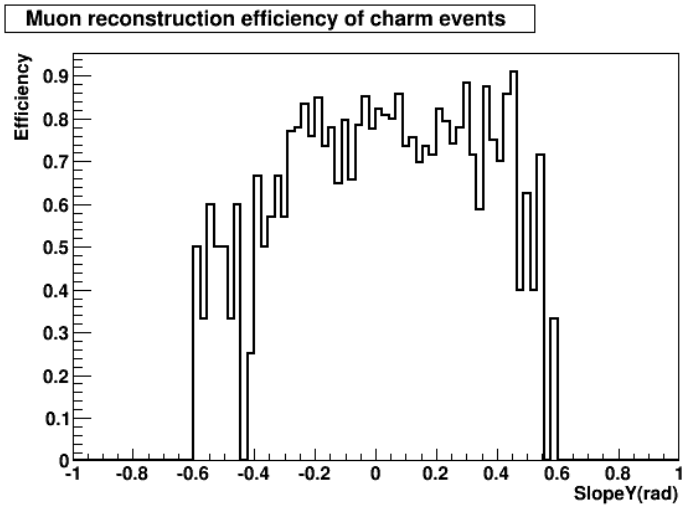

Figure 4.22: Muon reconstruction efficiency vs y slope for $\nu_\mu CC - Charm$.

4.3 The Track Purity in The Reconstructed Vertex

The purity of tracks belonging to the primary and secondary vertex is estimated comparing reconstructed vertex tracks with true vertex tracks. In $\nu_\mu CC$ events the purity is found to be 99%. This means that almost all primary tracks are real primary tracks. On the other hand, the purity is lower for $\nu_\mu CC - Charm$ events. It is found to be 67%. This means that there is a migration of tracks from secondary vertex to the primary vertex. This is significant for the short decay topology. In some cases, it is vice versa. That is the tracks of primary vertex can be clustered in the secondary vertex.

The primary vertex reconstruction efficiency for $\nu_\mu CC$ events is shown in Figure 4.23. The efficiency increases with the track multiplicity as expected. It becomes flat at prong 5.

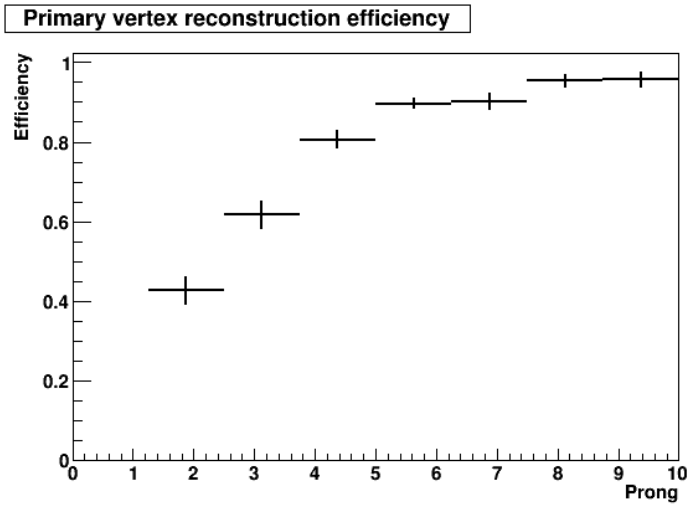

Figure 4.23: Primary vertex reconstruction efficiency vs prong.

The primary vertex reconstruction efficiency for $\nu_\mu CC - Charm$ events is shown in Figure 4.24. The reconstruction efficiency is higher than that of $\nu_\mu CC$ events. The main reason is that, the number of reconstructed tracks in $\nu_\mu CC - Charm$ events is higher than that of $\nu_\mu CC$ events.

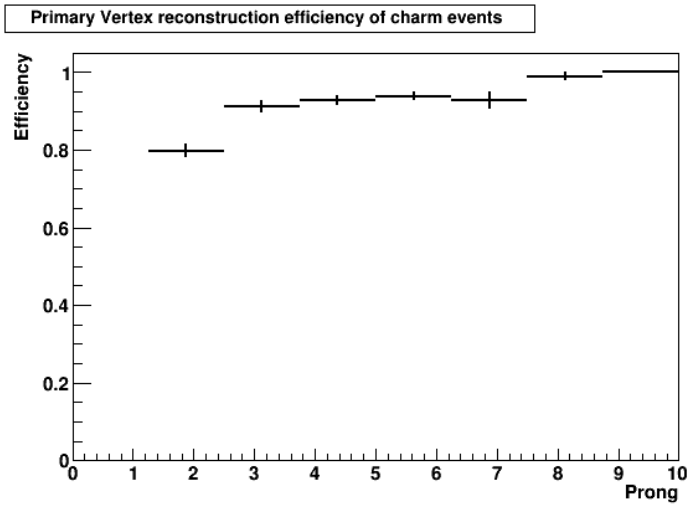

Figure 4.24: Primary vertex reconstruction efficiency vs prong for $\nu_\mu CC - Charm$.

CHAPTER 5

RESULTS

In this thesis, the reconstruction efficiency of ν_μ CC and ν_μ CC Charm events, based on neutrino energy, muon momentum, muon slope are estimated. These events, reconstructed by SYSAL package, are analyzed by an analysis code which is developed for this study. For ν_μ CC events reconstruction efficiency of primary vertex is found as 83.2% and in 73.8% primary vertex contains muon track. The main source of inefficiency is QE or RES type interactions. Since these interactions contain only one reconstructed track, namely muon, primary vertex cannot be reconstructed for this type of topologies. Another reason for inefficiency is large angle muons, which cannot found due to the scanning acceptance of the microscope.

The purity of decay topology in ν_μ CC events is found to be 99%. This means that almost all primary tracks are true primary tracks. The reconstruction efficiency of primary vertex and purity of ν_μ CC Charm events are estimated 90.2% and 73.9% respectively.

All physics results produced by the OPERA Collaboration are estimated using OpRelease framework. In this analysis, we have estimated the reconstruction performance of the reconstruction algorithm in OpRelease package. It is found that the single vertex topologies are reconstructed with high efficiency and purity. However, multi-vertex topologies have higher efficiency but lower purity due to mismatch of tracks. In some cases the true tracks of secondary vertex are clustered in the primary vertex. This also spoils the impact parameter distribution of the primary vertex track.

REFERENCES

[1] F. Reines and C. L. Cowan. Detection of the Free Neutrino. *Physical Review*, 92:830–831, 1953.

[2] G. Danby, J.-M. Gaillard, K. Goulianos, L. M. Lederman, N. Mistry, M. Schwartz, and J. Steinberger. Observation of High-Energy Neutrino Reactions and the Existence of Two Kinds of Neutrinos. *Physical Review Letters*, 9:36–44, 1962.

[3] DONUT Collaboration K. Kodama et al. et al. Observation of tau neutrino interactions. *Physics Letters B*, 504:218–224, 2001.

[4] R. M. et al Barnett. Review of Particle Physics. *Physical Review D*, 54:1–708, 1996.

[5] Y. Fukuda et al et al. Evidence for Oscillation of Atmospheric Neutrinos. *Physical Review Letters*, 81:1562–1567, 1998.

[6] S. Aoki et al et al. Indications of Neutrino Oscillation in a 250km Long-Baseline Experiment. *Physical Review Letters*, 90(4):041801, 2003.

[7] A. Strumia. Oscillations of three neutrinos with all Deltam^2 approx 10^{-3}eV^2. *Journal of High Energy Physics*, 4:26, 1999.

[8] G. Fiorentini, M. Lissia, G. Mezzorani, M. Moretti, and D. Vignaud. Solar neutrino experiments and determination of the neutrino oscillation parameters. *Physical Review D*, 49:6298–6318, 1994.

[9] T2K Collaboration. T2K experiment. *Nuclear Physics B Proceedings Supplements*, 145:178–181, 2005.

[10] D. Michael. The MINOS experiment. *Progress in Particle and Nuclear Physics*, 48:99–109, 2002.

[11] A. J. G. Hey I. J. R. Aitchison. *Gauge Theories in Particle Physics*. IOP Publishing, 2004.

[12] P. Watkins. *Story of the W and Z.* Cambridge University Press, 1986.

[13] B. Pontecorvo. Neutrino Experiments and the Problem of Conservation of Leptonic Charge. *Soviet Journal of Experimental and Theoretical Physics*, 26:984, 1968.

[14] M. Güler. *D^0 Production Rate Measurement in Neutrino Interactions and A limit on Muon Neutrino to Tau Neutrino Oscillations*. PhD thesis, Middle East Technical University, 2000.

[15] Z. Maki, M. Nakagawa, and S. Sakata. Remarks on the Unified Model of Elementary Particles. *Progress of Theoretical Physics*, 28:870–880, 1962.

[16] T. Schwetz, M. Tórtola, and J. W. F. Valle. Global neutrino data and recent reactor fluxes: the status of three-flavour oscillation parameters. *New Journal of Physics*, 13(6):063004, 2011.

[17] Main Sequence Stars. http://outreach.atnf.csiro.au/education/senior/astrophysics/, visited on January 5, 2012.

[18] R. Davis, D. S. Harmer, and K. C. Hoffman. Search for Neutrinos from the Sun. *Physical Review Letters*, 20:1205–1209, 1968.

[19] J. A. Thomas and P. L. Vahle. *Neutrino Oscillations, Present Status and Future Plans*. Singapore: World Scientific, 2007.

[20] S. L. Glashow, J. Iliopoulos, and L. Maiani. Weak Interactions with Lepton-Hadron Symmetry. *Physical Review D*, 2:1285–1292, 1970.

[21] K. Huang. *Fundamental Forces of Nature*. New Jersey: World Scientific, 2007.

[22] P. Migliozzi P. Santorelli G. De Lellis. Charm physics with neutrinos. Physics Reports 399, 2004.

[23] U. Dore. Physics with charm particles produced in neutrino interactions. A historical recollection. *ArXiv:1103.4572*, 2011.

[24] O. Melzer. *Study of charm production by neutrinos in nuclear emulsion*. PhD thesis, De Univeriteit van Amsterdam, 2001.

[25] S. Y. Tsai. Search for Color-Excitation in Single- and Di-Muon Neutrino-Production. *Progress of Theoretical Physics*, 59:214–226, 1978.

[26] A. Bodek. Status of the CCFR neutrino oscillation experiment at FNAL. In J. Tran Thanh van, editor, *Beyond the Standard Model, Volume 2*, page 77, 1983.

[27] A. Staude. First results from the CHARM II experiment. In J. Schneps, T. Kafka, W. A. Mann, & P. Nath, editor, *Neutrino Physics and Astrophysics*, page 397, 1988.

[28] A. Rubbia. Neutrino Oscillation MAgnetic Detector (NOMAD) Status Report Search for ν_τ appearance at the CERN SPS. *Nuclear Physics B Proceedings Supplements*, 40:93–107, 1995.

[29] T. Adams et al et al. Determination of $\sin^2\theta\_W$ from neutrino-nucleon scattering at NuTeV. *Nuclear Physics B Proceedings Supplements*, 77:265–270, 1999.

[30] M. Güler et al et al. Measurement of charm production in neutrino charged-current interactions. *New Journal of Physics*, 13(9):093002, 2011.

[31] N. Agafonova et al. et al. Observation of a first $\nu\_$ candidate event in the OPERA experiment in the CNGS beam. *Physics Letters B*, 691:138–145, 2010.

[32] R. Acquafredda et al. et al. The OPERA experiment in the CERN to Gran Sasso neutrino beam. *Journal of Instrumentation*, 4:4018, 2009.

[33] SPS CNGS. https://accstat.web.cern.ch/accstat/statistics/charts/2011/sps, visited on December 16, 2011.

[34] M. Güler et al et al. OPERA Experiment Proposal. CERN/SPSC 2000-028, LNGS P25/2000.

[35] S. Tufanlı. D^0 background to neutrino oscillations in the OPERA Experiment. Master's thesis, Middle East Technical University, 2009.

[36] L. Arrabito et al. et al. Hardware performance of a scanning system for high speed analysis of nuclear emulsions. *Nuclear Instruments and Methods in Physics Research A*, 568:578–587, 2006.

[37] M. De Serio et al. et al. High precision measurements with nuclear emulsions using fast automated microscopes. *Nuclear Instruments and Methods in Physics Research A*, 554:247–254, 2005.

[38] Bart Van de Vyver. *Determination of the semi-leptonic branching fraction of neutrino-induced charm hadrons using nuclear emulsion*. PhD thesis, Vrije Universiteit Brussel, 2002.

[39] L. Chaussard. OpGeom: software model of the OPERA detector. *OPERA Internal Notes 69*, 2005.

[40] A. Marotta OPERA Presentation. http://indico.cern.ch/contribid=36confid=13356, visited on June 24, 2011.

[41] CMT web page. http://www.cmtsite.org/, visited on November 20, 2011.

[42] CERNLIB we page. http://cernlib.web.cern.ch/cernlib/, visited on November 22, 2011.

[43] CLHEP web page. http://proj-clhep.web.cern.ch/proj-clhep/, visited on November 22, 2011.

[44] ROOT web page. root.cern.ch/, visited on November 22, 2011.

[45] Pythia6 web page. http://projects.hepforge.org/pythia6/, visited on November 22, 2011.

[46] ORACLE web page. http://www.oracle.com/index.html, visited on November 22, 2011.

[47] OpRelease web page. http://operaweb.lngs.infn.it/operawiki/index.php/OpRelease, visited on July 10, 2011.

[48] S. Dusini. How to access data but also MC in OpEmuRec. *OPERA Workshop*, 2010.

[49] V. Tioukov, I. Kreslo, Y. Petukhov, and G. Sirri. The FEDRA-Framework for emulsion data reconstruction and analysis in the OPERA experiment. *Nuclear Instruments and Methods in Physics Research A*, 559:103–105, 2006.

[50] C. Bozza et al. SySal: System of Salerno. *ArXiv:hep-ex/9901031*, 1999.

[51] M. Besnier et al. Vertex reconstruction studies with FEDRA and performances on hadronic multivertex neutrino events. *OPERA Interal Notes*, 2007.